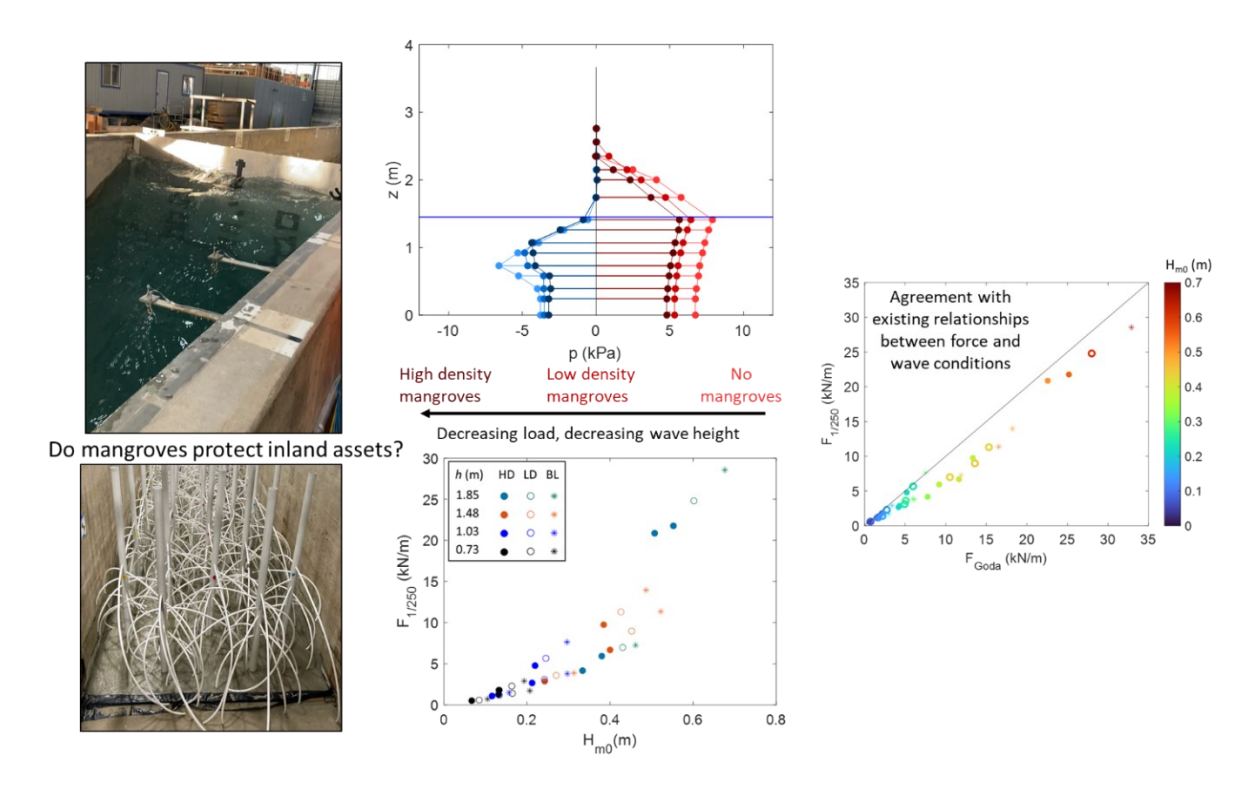
1 2 3	Prototype-scale Laboratory Observations of Wave Force Reduction by an Idealized Mangrove Forest of Moderate Cross-shore Width			
4	Tori Tomiczek <sup>1*</sup> , William T. Mitchell <sup>2</sup> , Pedro Lomónaco <sup>3</sup> , Daniel Cox <sup>4</sup> , Kiernan Kelty <sup>5</sup>			
5 6 7 8 9 10 11 12 13 14 15 16 17 18 19	<ul> <li>Department of Naval Architecture and Ocean Engineering, United States Naval Academy, Annapolis, MD 21402, vjohnson@usna.edu.</li> <li>U.S. Naval Facilities Engineering Command, 1322 Patterson Ave, SE, Suite 1000, Washington Navy Yard, D.C., 20374, USA. william.t.mitchell136.mil@us.navy.mil.</li> <li>O.H. Hinsdale Wave Research Laboratory, Oregon State University, 3550 SW Jefferson Way, Corvallis, OR 97331, USA. pedro.lomonaco@oregonstate.edu.</li> <li>School of Civil and Construction Engineering, Oregon State University, Corvallis, OR 97331, dan.cox@oregonstate.edu.</li> <li>cbec, Eco Engineering, 519 Seabright Ave, Suite 102, Santa Cruz, CA 95062, USA. k.kelty@cbecoeng.com.</li> <li>*Corresponding author: vjohnson@usna.edu</li> <li>Highlights</li> </ul>			
20	A model mangrove forest reduced wave heights and wave forces on a vertical wall.			
21	2. For random waves the 18 m forest reduced $1/250$ characteristic forces by $4-43\%$ .			
22	3. Attenuated wave heights in existing equations gave very good wave force estimates.			
23	4. Seaward wave forces were similar or greater than shoreward forces for some trials.			
24	5. Results inform engineering guidance for implementing mangrove forests in design.			
25	Abstract			
26	A prototype-scale physical model was used to study wave height attenuation through an			
27	idealized mangrove forest and the resulting reduction of wave forces and pressures on a vertical			
28	wall. An 18 m transect of a <i>Rhizophora</i> forest was constructed using artificial trees, considering			
29	a baseline and two mangrove stem density configurations. Wave heights seaward, throughout,			
30	and shoreward of the forest and pressures on a vertical wall landward of the forest were			
31	measured. Mangroves reduced wave-induced forces by 4% to 43% for random waves and 2% to			
32	38% for regular waves. For nonbreaking wave cases, the shape of the pressure distribution was			

consistent, implying that the presence of the forest did not change wave-structure interaction
processes. Analytical methods for determining nonbreaking wave-induced loads provided good
estimations of measured values when attenuated wave heights were used in equations. The ratio
of negative to positive force ranged between 0.14 and 1.04 for regular waves and 0.31 to 1.19 for
random waves, indicating that seaward forces can be significant and may contribute to
destabilization of seawalls during large storms. These results improve the understanding of
wave-vegetation-structure interaction and inform future engineering guidelines for calculating
expected design load reductions on structures sheltered by emergent vegetation.

### 47 Graphical Abstract



**Keywords**: *Rhizophora mangle* (red mangroves), wave-induced forces, physical modeling, nature-based solutions, engineering with nature, coastal flood hazard mitigation

#### 1. Introduction

As coastal communities face increasing exposure to coastal flood hazards, support has grown for leveraging existing or restored natural ("green") infrastructure systems in combination with, or as alternatives to, conventional ("gray") infrastructure systems for coastal flood hazard mitigation. Natural infrastructure systems (*e.g.*, vegetation, beaches and dunes, reefs), also referred to as Natural and Nature-Based Features (NNBF), Nature-based Solutions (NbS), Building With Nature (BWN), Engineering With Nature (EWN), among other terms, can provide engineering, environmental, economic, and social benefits when implemented properly. As a result, major initiatives have sought to implement these systems more broadly at local and

62

63

64

65

66

67

68

69

70

71

72

73

74

75

76

77

78

79

80

81

82

83

regional scales (Hardaway et al. 2017, Turconi et al. 2020) and at national and international scales (Bridges et al. 2021, NOAA 2015, Faivre et al. 2017, Webb et al. 2019, World Bank 2017, Castellari et al. 2021). Efforts have proposed guidelines for restoring or conserving natural infrastructure in coastal environments (NOAA 2015, Webb et al. 2019, Bridges et al. 2021, Bredes et al. 2023) and considering changes over a natural system's growth cycle (Maza et al. 2021, Ostrow and Cox, submitted). However, quantitative and robust design guidelines at a similar rigor to manuals of practice and design standards for conventional systems (e.g., ICC 2015, USACE 2002, ASCE 2022) are required in order to confidently incorporate these systems in coastal protection design. Knowledge gaps in the quantitative engineering performance of natural infrastructure systems must be bridged in order to develop rigorous technical standards for these systems' design, construction, and adaptive management (Ostrow et al. 2022). Wetlands comprising native emergent vegetation (e.g., maritime forests, mangroves, marsh vegetation) represent a natural infrastructure solution with potential to mitigate coastal hazards in a wide range of climates. In tropical and subtropical regions, mangrove forests dominated by the *Rhizophora* genus, characterized by their dense network of above-ground prop roots, have been observed to mitigate surge or long wave effects in near-shore communities over sufficiently large spatial scales (Danielsen et al. 2005, Zhang et al. 2012, Rahdarian and Niksokhan 2017, Goda et al. 2019) and to reduce damages due to storm waves over moderate cross-shore distances (Tomiczek et al. 2020a). In addition to post-event observations, laboratory experiments (Chang et al. 2019, Maza et al. 2019, Keimer et al. 2021, Kelty et al. 2022, Wang et al. 2022a, 2022b, Yin et al. 2020, 2023, Zhang et al. 2023), numerical investigations (Wang et al. 2020, Yin et al. 2020, 2024), and field measurements (Mazda et al. 1997, Horstman et al. 2014, Tomiczek et al. 2022) have shown that mangroves or other idealized vegetation can attenuate

wave heights over large and moderate spatial scales during storm conditions or under operational stressors such as vessel-generated wakes. Reduced-scale physical model experiments (Tomiczek et al. 2020b, Van Dang et al. 2023, Chen et al. 2023) and computational simulations (Rosenberger and Marsooli 2022) have also demonstrated wave-induced load reduction on structures sheltered by idealized mangrove forests or coastal forest "green belts" (Fathi-Moghadam et al. 2018), which may lead to avoided damages to near-coast structures during overland flow events. Numerical modeling efforts have similarly shown that mangroves can reduce wave energy and lead to avoided losses to the built environment during storm events (Guannel et al. 2016, Menéndez et al. 2020).

While these studies have advanced the understanding of the performance of mangrove forests in ameliorating coastal flood hazards over a range of incident conditions, the focus has been primarily on quantifying wave height reduction or qualitatively observing post-storm impacts in the built environment. Few studies have investigated the effects of mangrove forests on reducing loads on sheltered near-coast structures (Tomiczek et al. 2020b, Van Dang et al. 2023, Chen et al. 2023), with previous measurements based on reduced-scale physical models subject to transient (tsunami-like) waves rather than random wave conditions expected during storm events. While reduced-scale experiments provide useful information about wave-vegetation-structure interaction, careful interpretation is needed to ensure that results are appropriately applied at prototype scales (Kelty et al. 2022). Therefore, measurements of load reduction by natural infrastructure systems interacting with wind waves at prototype-scale are necessary to inform performance criteria for existing design standards and manuals of practice.

Several methodologies already exist for predicting wave-induced loads on near-coast structures. For example, the *Coastal Engineering Manual* (USACE 2002) presents equations for

108

109

110

111

112

113

114

115

116

117

118

119

120

121

122

123

124

125

126

127

128

129

predicting wave forces on structures based on parameters including structure geometry, incident wave height, wavelength, and water depth, among others (Sainflou 1928, Goda, 1974, Tanimoto et al. 1976). A well-accepted methodology for predicting wave forces on walls is based on the method proposed by Goda (2010) for determining the wave-induced pressure distribution on a caisson breakwater. Wiebe et al. (2014) showed that this method can be modified for vertical walls of near-coast elevated structures such as residential buildings, and Tomiczek et al. (2019) later validated these equations for elevated structures based on large-scale experiments. This method was adopted by the American Society of Civil Engineers (ASCE) as prescriptive for determining wave loads on buildings and other structures (ASCE 2022). Other equations have been proposed to determine impulsive and quasi-static wave forces on walls (Blackmore and Hewson 1984, Cuomo et al. 2010). However, despite the advancement of analytical methods for predicting wave height attenuation through vegetation (NAS 1977, Dalrymple et al. 1984, Mendez and Losada 2004, Kelty et al. 2022), the applicability of existing design equations for computing the wave-induced force on structures due to waves that have propagated through shielding vegetation remains unknown.

Therefore, the objectives of this paper were to (1) assess the capacity of mangrove systems to mitigate wave-induced loads in the built environment under various wave and mangrove density conditions, and (2) incorporate wave-vegetation interaction (*i.e.*, wave height decay through mangrove forests) into analytical equations for wave force prediction to assess the ability of existing methods for predicting wave-induced loads on near-coast structures sheltered by vegetation. This study investigated these research objectives through construction and testing of a prototype-scale physical model of an idealized mangrove forest to measure wave height attenuation and pressures (forces) on a vertical wall sheltered by vegetation. The remainder of

the paper is structured as follows: Section 2 presents details of the physical model experiment, including descriptions of the facility, instrumentation, configurations, and wave conditions tested during experiments. Section 3 describes results and observations of mangrove effects on wave-induced loads for regular and random wave conditions, and comparisons of measured forces with predicted forces from existing analytical methods. Section 4 discusses implications of these experiments within the context of nature-based solutions and engineering design and identifies opportunities for future research. Section 5 presents the main conclusions of the study.

### 2. Laboratory Investigation

2.1 Experimental Facility, Test Specimens, Instrumentation, and Wave Conditions

Experiments were performed in the Large Wave Flume (LWF) of the O.H. Hinsdale Wave Research Laboratory at Oregon State University. The flume was 104 m long x 3.66 m wide x 4.6 m high, with a maximum water depth of 2.74 m. The flume was equipped with a piston-type wavemaker with a maximum stroke of 4 m and was capable of generating regular, irregular, tsunami-like, and user-defined waves. The coordinate system was defined with x-, y-, and z- axes indicating the cross-shore, alongshore, and vertical directions, respectively. The origin (x = y = z = 0) was at the neutral position of the wavemaker in the x-direction, flume centerline in the y-direction, and base of the flume in the z-direction. For these experiments, the bathymetry was constructed as shown in the profile drawing seen in Fig. 1; upon generation, waves propagated across a 17.93 m long horizontal section before reaching a 7.32 m long 1:12 slope. Following the crest of the slope, at x = 25.25 m, waves propagated across a 36.61 m long horizontal test section comprising an 10.99 m section to characterize incident waves, followed by an 18.28 m long test section where the idealized mangrove forest was installed (Fig. 1c), and

finally a 7.34 m long horizontal section between the shoreward edge of the idealized mangrove forest and an instrumented vertical wall positioned at x = 61.86 m.

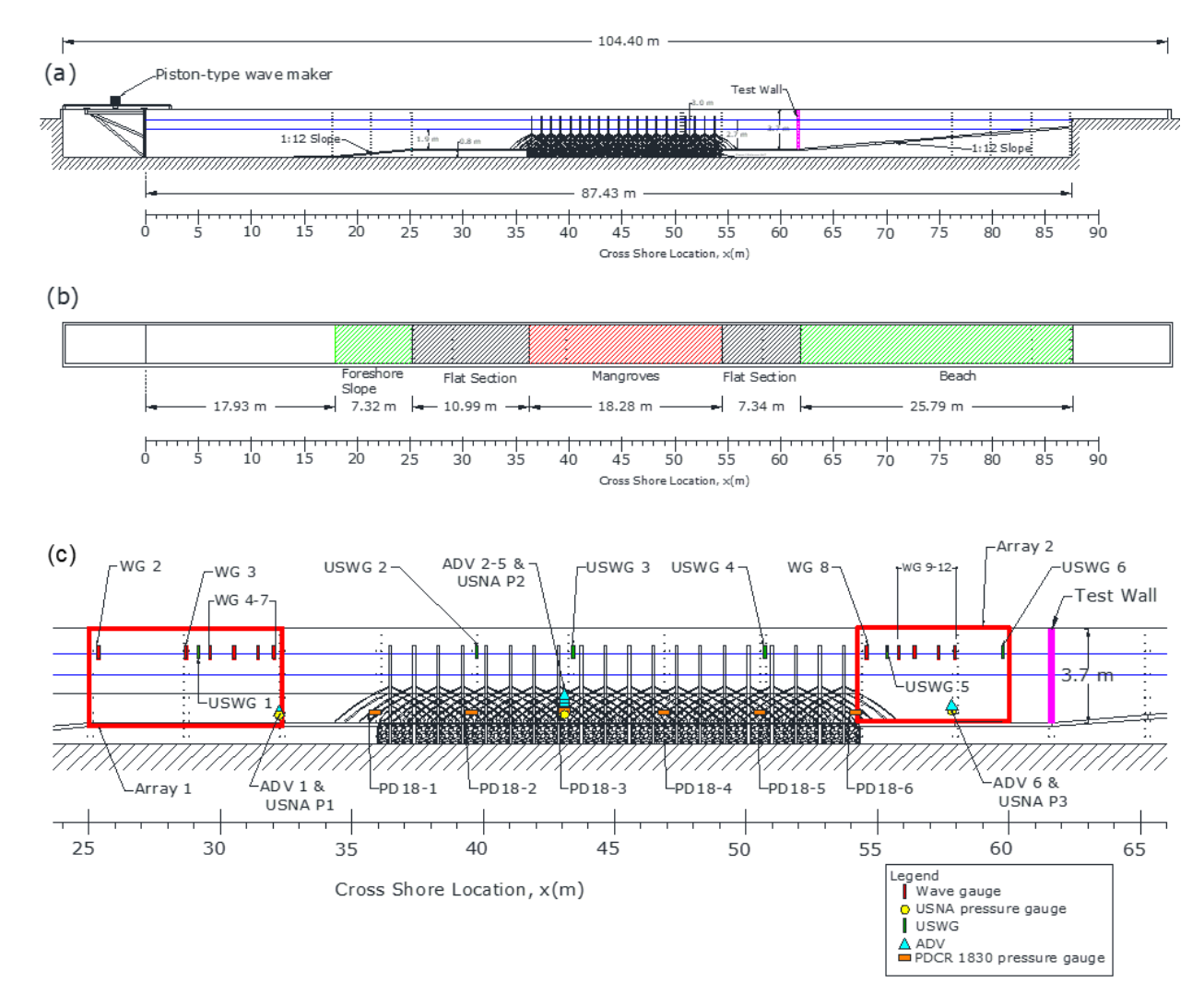
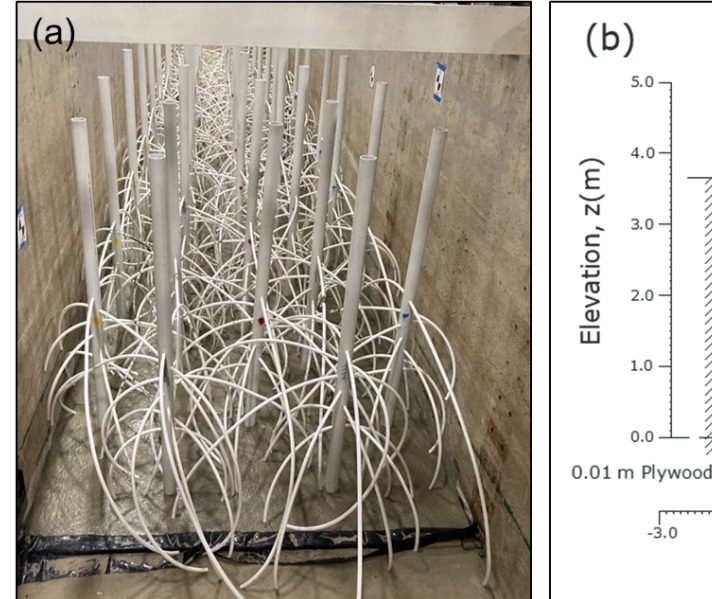


**Figure 1:** (a) Profile view and (b) plan view of experimental configuration and layout in the Large Wave Flume, showing bathymetry and location of mangrove forest section; (c) profile view of mangrove test section showing locations of instrumentation and wall.

The idealized mangrove specimens (Fig. 2a) were constructed based on the trunk-prop root system of the *Rhizophora* genus. Individual specimen designs were parameterized using the model proposed by Ohira et al. (2013), modified for constructability similarly to previous reduced-scale studies (Tomiczek et al. 2020b, Bryant et al. 2022). The specimens were the same

as those used by Kelty et al. (2022) and were constructed using polyvinyl chloride (PVC) pipe for trunks and cross-linked polyethylene (PEX) for prop roots. Each specimen had a diameter at breast height  $D_{BH} = 0.1143$  m and 14 prop roots with diameter  $D_{Root} = 0.0286$  m. These dimensions are consistent with reported values from field measurements of *Rhizophora mangle* and other mangrove species in south Florida and the Caribbean (Jimenez et al. 1985, Dawes et al. 1999, Novitzky 2010, Loría-Naranjo et al. 2014). Root length increased with elevation above the ground; roots were installed in pairs at seven vertical locations with the lowest and highest roots elevated 0.58 m and 1.35 m above ground and extending 0.67 m and 2.10 m from the base of the tree, respectively. Individual specimens, including prop roots, were secured to the flume bottom using construction sand and a 0.076 m concrete cap (Fig. 2b). Additional details on the mangrove specimen design are presented in Kelty et al. (2021, 2022).





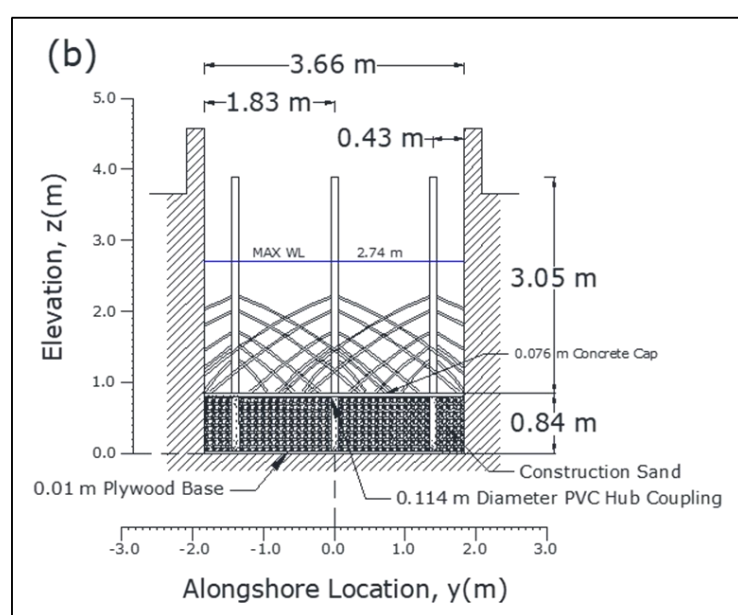


**Figure 2:** (a) Photograph of high-density mangrove test section; (b) forest cross section drawing showing anchoring of mangrove specimens.

Mangrove effects on wave-induced force reduction were assessed by measuring the wave-induced pressures on a vertical wall positioned 7.34 m shoreward of the mangrove forest section at x = 61.86 m. A detailed drawing of the wall is presented in Fig. 3a, and photographs of the wall installed in the flume and from the shoreward edge of the mangrove forest are shown in Fig. 3b and Fig. 3c, respectively. The wall was constructed using two aluminum sections each measuring 3.66 m wide x 1.83 m high, and the total wall height was 3.66 m. The wall was secured to the sides of the flume, and a rubber seal was installed between the aluminum plates and flume sidewalls to prevent flow past the sides of the wall. Seals were created between the bottom wall section and the floor and between the upper and lower wall sections using wooden boards and waterproof tape. The wall deformation was not measured during these tests.



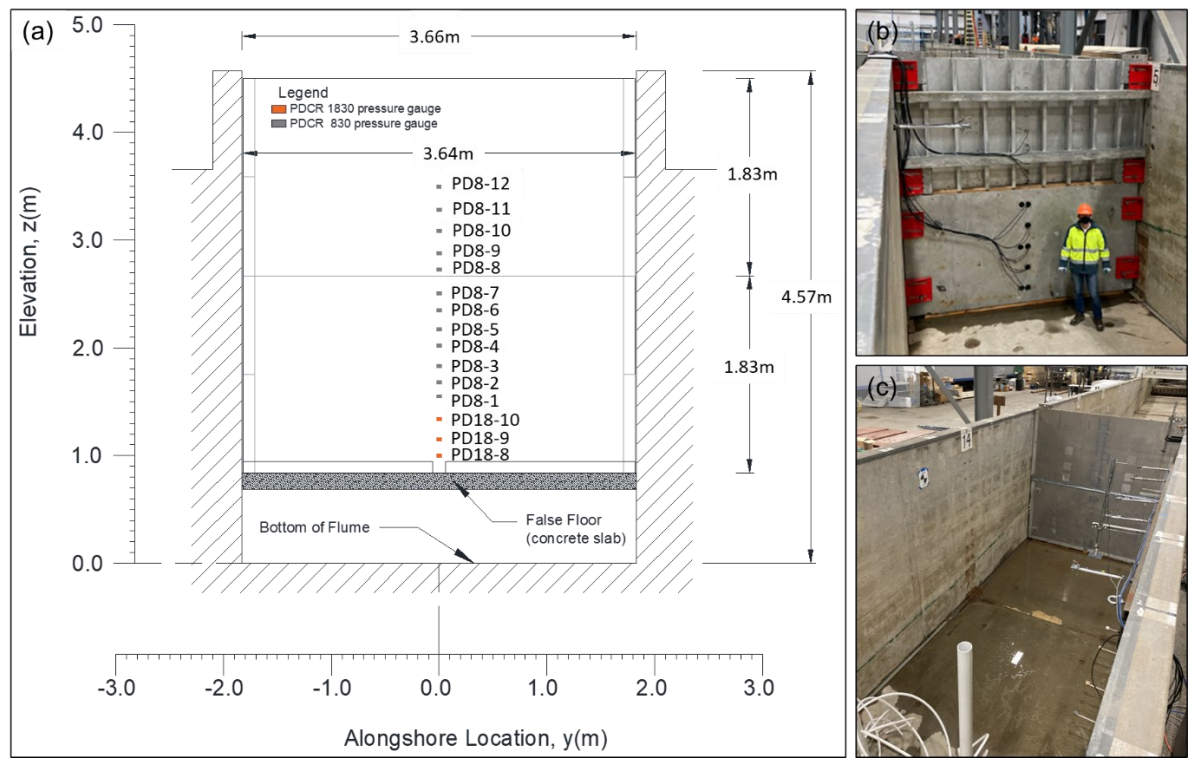


**Figure 3:** (a) Wall cross-section view showing locations of pressure gauges; (b) photograph of wall during pressure gauge installation; (c) photograph of wall from shoreward edge of mangrove forest.

Six test layouts were considered for experiments as presented in Table 1 (Kelty et al., 2021). Waves were generated for three configurations with and without the instrumented wall. Configurations included a baseline (BL) configuration and mangrove configurations considering two forest stem densities installed along the 18 m test section shown in Fig. 1c. Reported forest densities at field sites in Florida and the Caribbean range from 0.112 stems/m² to 2.02 stems/m² (Jimenez et al. 1985, Dawes et al. 1999, Novitzky 2010, Loría-Naranjo et al. 2014). The experiments classified mangrove configurations with stem densities of 0.375 stems/m² as low-density (LD) and 0.75 stems/m² as high-density (HD) representing a mature, homogeneous mangrove forest. The present study focuses on those layouts including the wall (Layouts 2, 3, and 6 in Table 1). Wave height attenuation through the forest with no wall (Layouts 1, 4, and 5) were analyzed in Kelty et al. (2022).

**Table 1.** Experimental test layouts

Layout	Configuration	Wall	
1	High-Density (HD)	No	
2	High-Density (HD)	Yes	
3	Low-Density (LD)	Yes	
4	Low-Density (LD)	No	
5	Baseline* (BL)	No	
6	Baseline* (BL)	Yes	
*No mangroves			

Instrumentation used in this experiment to measure wave characteristics throughout the

experimental test section included wire resistance wave gauges (WGs), ultrasonic wave gauges (USWGs), acoustic Doppler velocimeters (ADVs), and, within the mangrove forest, submerged PDCR 1830 pressure gauges (PD18s), which were corrected to the free surface accounting for

dynamic wave pressure attenuation with depth. Locations of instruments positioned seaward,

throughout, and shoreward of the forest test section are shown in Fig. 1c. Additional pressure gauges were installed along the centerline of the wall to measure wave-induced pressures. These sensors included three PDCR 1830 pressure gauges (PD18s) and twelve PDCR 830 pressure gauges (PD8s), which are denoted as orange and gray rectangles in Fig. 3a, respectively. This study focuses on analysis of the PDCR pressure gauge data to determine wave forces. The sampling rate for all hydrodynamic and load instrumentation was 100 Hz. This frequency is sufficient to measure quasi-static loads; short-duration, impulsive pressures from breaking waves require much higher sampling rates (e.g., Bullock et al. 2007, Cuomo et al. 2010, Park et al. 2017), and were not the focus of this study. Instruments were synchronized to the start of the time series of the wavemaker displacement. Instrumentation coordinates for WGs, USWGs, ADVs, PD18s recording hydrodynamics through the mangrove test section are provided in Appendix Table A.1, and instrumentation coordinates for PD18s and PD8s measuring pressures on the wall are provided in Appendix Table A.2.

Four water depths were considered in experiments, with water depths at the vegetation test section  $h_v = 1.85$  m, 1.48 m, 1.03 m, and 0.73 m. Initially, three water depths were selected to represent varying storm surge conditions within the root system ( $h_v = 0.73$  m and 1.03 m) or above the root system ( $h_v = 1.85$  m), allowing for comparison of the effects of the projected area of the vegetation on wave height attenuation (Kelty et al. 2022). The intermediate water depth  $h_v = 1.48$  m (above the root system) was added for the LD and BL configurations (Layouts 3-6) due to increased time available at the facility for testing. However, trials for the HD configuration were not repeated at this water depth because of the schedule for the mangrove specimen installation and removal. A total of 23 regular, 11 random and 6 transient (tsunami-like) wave cases with varying incident parameters (*i.e.*, wave height, period, water depth) were generated

for each layout, and the wave transformation through the mangrove forest section and resulting pressures (forces) on the wall were measured. The data from these experiments for all wave cases and experimental configurations were published by Kelty et al. (2021). This study focuses on analysis of regular and random wave conditions generated for the wall configurations, with an emphasis on nonbreaking and quasi-static wave forces on with the wall and does not present results of transient wave cases. Figures 4 and 5 show plots of relative wave height (wave height divided by water depth at the vegetation,  $H/h_{v/}$ ) vs. relative water depth (water depth at the vegetation divided by wavelength,  $h_{v/}L$ ) measured at Array 2, which was located shoreward of the mangrove forest and seaward of the wall, for regular and random wave conditions, respectively. Wave heights and periods were varied for the four water depths to consider six non-dimensional cases of relative wave height and relative water depth for regular wave conditions and three non-dimensional cases for random wave conditions. The figures also show curves indicating boundaries of wave breaking, various wave theories and classifications as shallow, intermediate, or deep-water wave conditions.

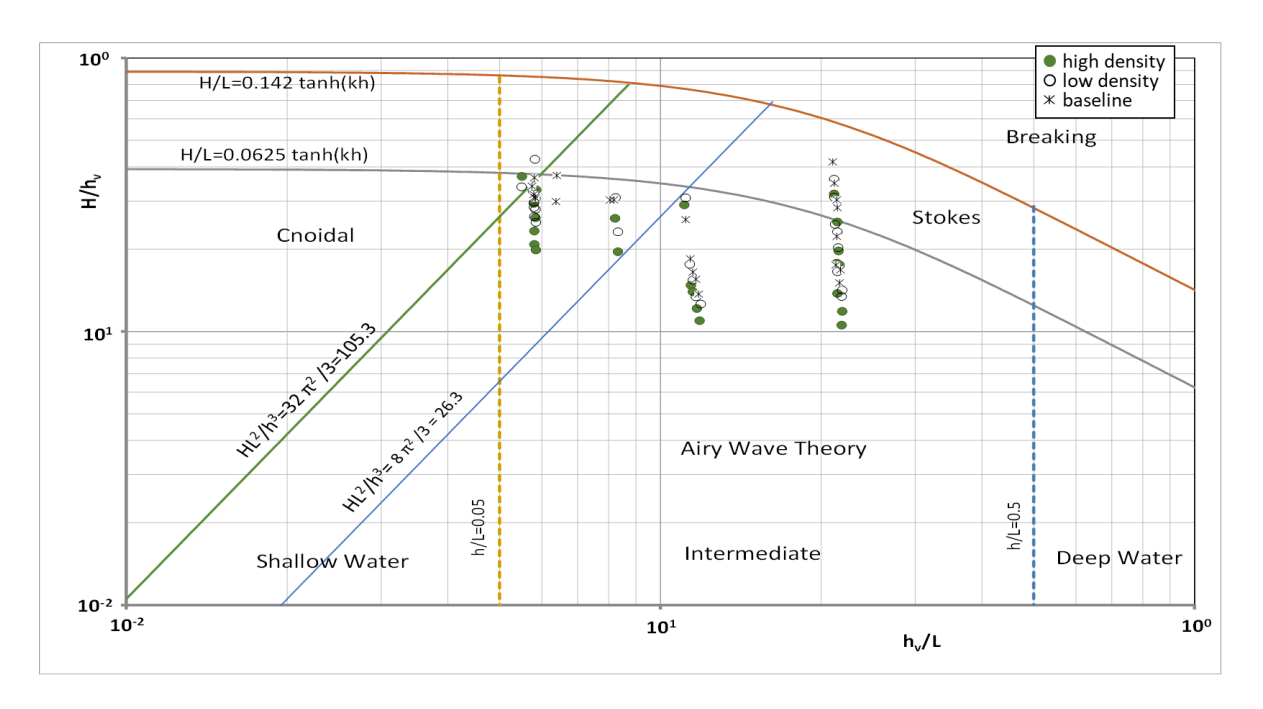


**Figure 4:** Regular wave conditions' relative wave height  $H/h_v$  vs. relative water depth  $h_v/L$ , measured at Array 2 for baseline (asterisks), low-density forest (hollow circles), and high-density forest (filled circles) configurations.

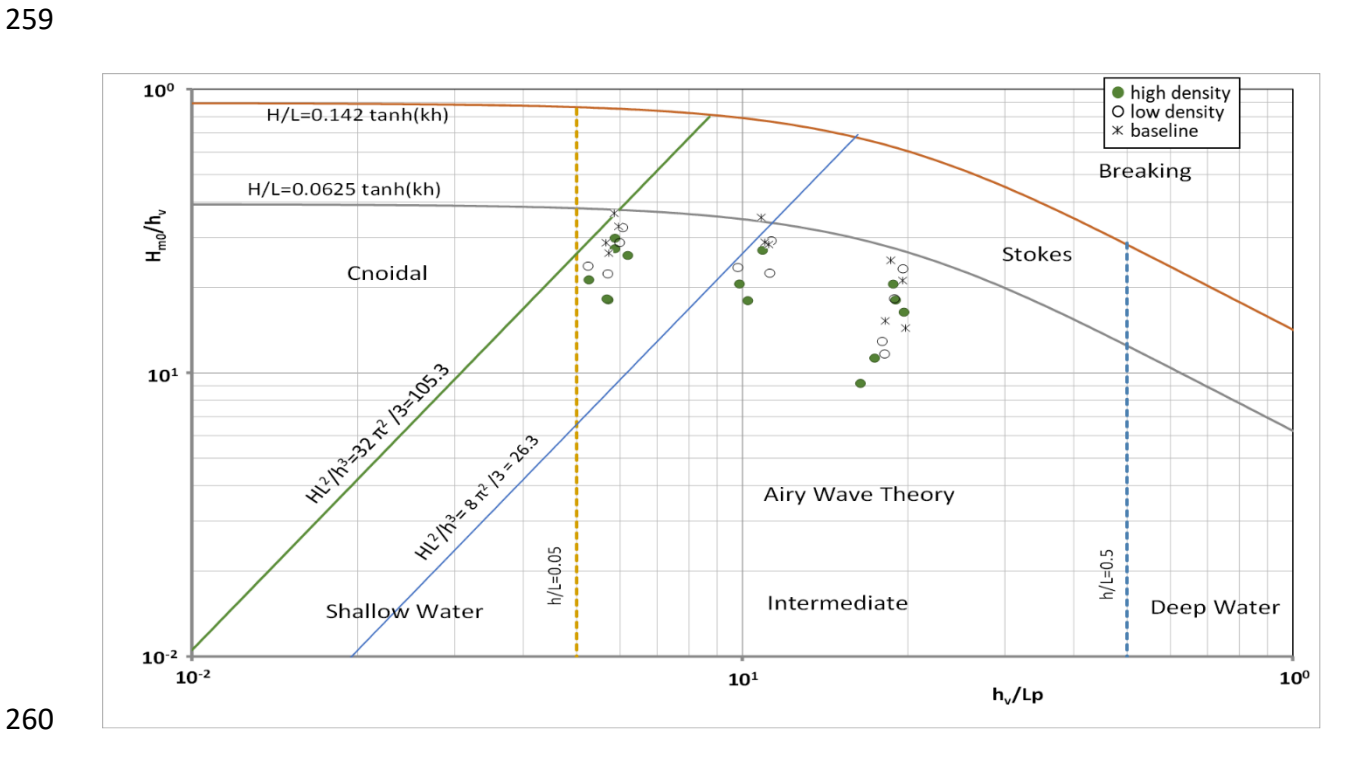


**Figure 5:** Random wave conditions' relative significant wave height  $H_{m0}/h_v$  vs. relative water depth  $h_v/L$ , measured at Array 2 for baseline (asterisks), low-density forest (hollow circles), and high-density forest (filled circles) configurations.

As indicated in Fig. 4 and Fig. 5, wave heights and periods were selected to create
conditions ranging from typical wave environments to more extreme storm-driven waves for
coastal areas where mangroves are present (Marsooli and Lin, 2018, Heidarzadeh et al. 2018,
Tomiczek et al. 2020a). For regular waves, 20 individual waves were generated plus additional
waves for ramp up and ramp down. Measured wave heights $H$ at PD18-1, located at the fringe of
the mangrove forest at $x = 35.89$ m from the wavemaker (Fig. 1c) ranged from 0.15 m ( $h_v = 1.03$
m) to 1.21 m ( $h_v = 1.48$ m), and wave periods T ranged from 1.86 s to 7.80 s. For each random
wave trial, 300 individual waves were generated using a JONSWAP spectrum with $\gamma = 3.3$ .
Measured spectral significant wave heights $H_{m0}$ at PD18-1 ranged from 0.10 m ( $h_v = 0.73$ m) to
0.73 m ( $h_v = 1.85$ m), and peak wave periods $T_p$ ranged from 1.58 s to 7.45 s. While wave
breaking was observed in some regular and random wave trials, the goal was to generate waves
that did not break under depth- or steepness-limited conditions to measure wave height and load
dissipation caused by the presence of the HD or LD mangrove forest configurations. Figure 6
shows example photographs of waves interacting with the mangrove forest and wall for various
water depths and wave conditions.

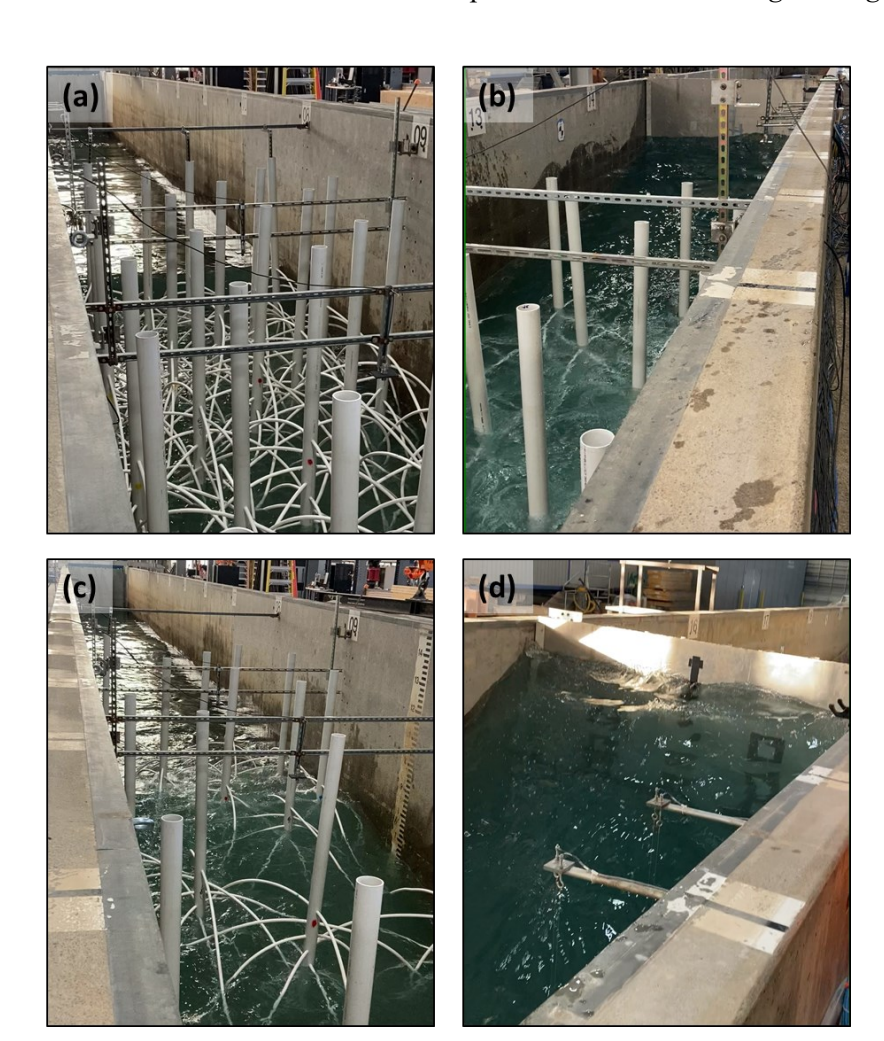


**Figure 6:** Photographs of wave-mangrove-wall interaction: (a), (b) high-density (HD) configuration for (a)  $h_v = 0.73$  m, view through forest section towards the wave maker and (b)  $h_v = 1.85$  m, view of wave-wall interaction; (c), (d) low-density (LD) configuration for (c)  $h_v = 1.03$  m, view through forest section towards the wave maker and (d)  $h_v = 1.85$  m, view of wave-wall interaction.

2.2 Data Processing and Ensemble Averages for Free Surface and Load Measurements

287

288

289

290

291

292

293

294

295

296

297

298

299

300

301

302

303

304

305

306

307

Water surface elevation data from WGs positioned at Arrays 1 and 2 (seaward and shoreward of the mangrove forest test section, respectively, Fig. 1c) were separated into incident and reflected free surface time series using the Wavelab 3 software developed by Aalborg University (Frigaard and Lykke Andersen 2014). The software performs the analysis based on methods presented by Zelt and Skielbreia (1992) for linear waves and Andersen et al. (2017) for nonlinear waves, with cross-mode separations performed following Gronbech et al. (1997). The incident wave time series measured at Array 2 for each trial was used in subsequent analysis of wave forces, omitting ramp-up and ramp-down portions of the signal to determine characteristic mean wave height  $\overline{H}$  and wave period  $\overline{T}$ . For regular waves, where variation in the free surface was observed due to factors such as wave breaking, the portion of the time series considered was that for which two times the standard deviation in wave heights was within 5% or 15% of the average wave height for nonbreaking or breaking waves, respectively. Examples of the total, reflected, and incident water surface elevation time series at Array 2 for the baseline configuration (no mangroves) are shown for selected wave conditions in Fig. 7a (case TR-h4-2,  $h_v = 0.73 \text{ m}, \overline{H} = 0.100 \text{ m}, \overline{T} = 2.51 \text{ s}$ ) and Fig. 7c (case TR-h1-4,  $h_v = 1.85 \text{ m}, \overline{H} = 0.587 \text{ m}, \overline{T} = 0.587 \text{ m}$ 7.66 s). The time series of force per unit width on the wall was determined using trapezoidal integration of the pressure gauge time series vertically up the face of the wall. Force time series corresponding to the free surface time series shown in Fig. 7a,c were plotted as shown in Fig. 7b,d, respectively.

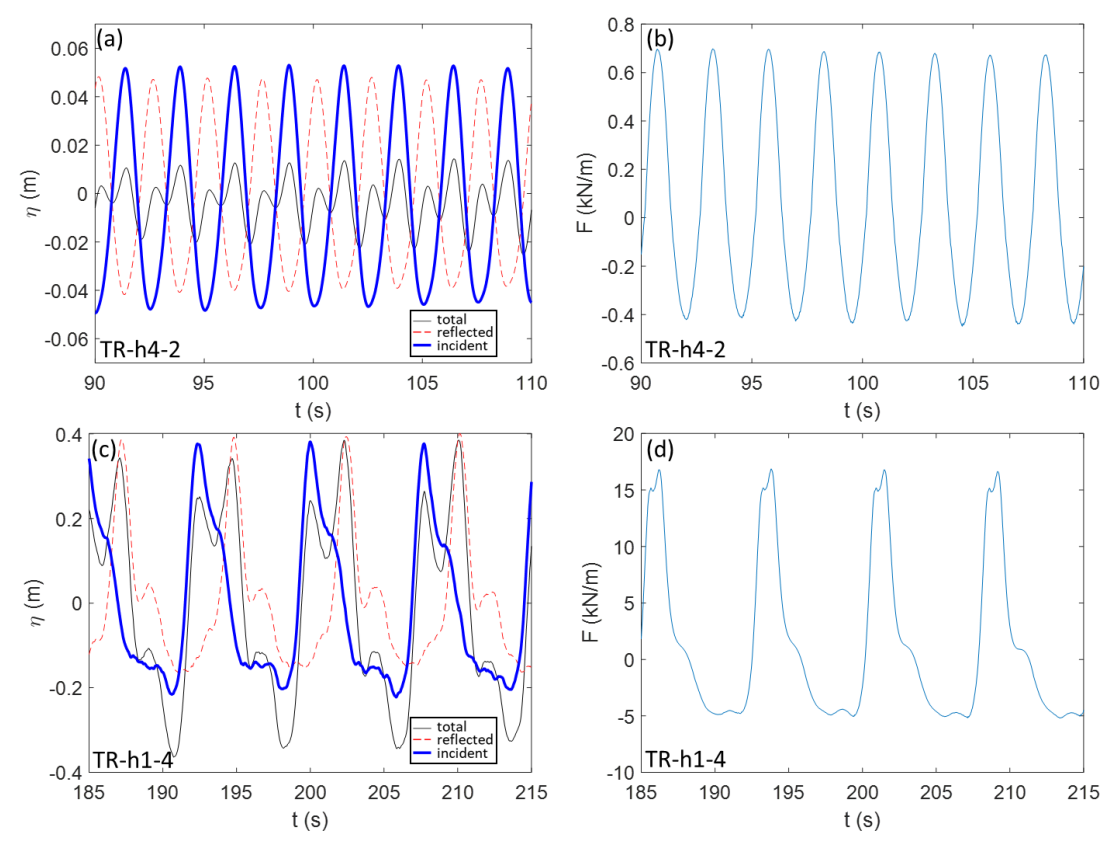


**Figure 7:** Example time series of total (black), reflected (dashed red), and incident (thick blue) free surface (a), (c) and corresponding force per unit width (b), (d) for Layout 6 (Baseline) for wave conditions (a), (b) TR-h4-2,  $h_v = 0.73$  m,  $\overline{H} = 0.100$  m,  $\overline{T} = 2.51$  s; and (c), (d) TR-h1-4,  $h_v = 1.85$  m,  $\overline{H} = 0.587$  m,  $\overline{T} = 7.66$  s.

For each water surface and force time series for regular waves, a LOESS filter (Marsh 2024) was applied to compute the ensemble average water surface and force time series using *Matlab* (2021). Figure 8a and 8c show examples phase-averaged water surface elevations, and Fig. 8b and 8d show the corresponding phase-averaged forces from two wave conditions for the baseline (black with 95% confidence intervals shaded in grey), low- (red dashed), and high-density (blue dash-dot) layouts. In general, the majority of the trials resulted in non-breaking wave conditions at Array 2, which was located just seaward of the wall, resulting in good agreement between repeated trials (*e.g.*, Fig. 8a, b). For trials where breaking or high wave nonlinearities occurred, greater variation was observed in ensemble averages of the free surface

and wave-induced force. As seen in Fig. 8, the ensemble average water surface elevation and force generally decreased as the mangrove stem density increased from the baseline to the lowand then to the high-density configuration. These results are consistent with measurements from other regular wave trials, for which the average maximum wave-induced force,  $\overline{F_+}$ , average maximum negative wave-induced force,  $\overline{F_-}$ , 95% confidence intervals ( $\overline{F_+}$  95% CI and  $\overline{F_-}$  95% CI, respectively), and elevation above the bed z at which the resultant shoreward or seaward forces were applied ( $\overline{Z_{F+}}$  and  $\overline{Z_{F-}}$ , respectively) are reported in Appendix Table B.1 along with hydrodynamic conditions for each wave case (water depth,  $h_v$ , ensemble average wave height,  $\overline{H}$ , 95% confidence interval,  $\overline{H}$  95% CI, and ensemble average period,  $\overline{T}$ ) and configuration (HD, LD, or BL). While in few cases the transmitted wave height for the baseline configuration was similar or slightly smaller than those recorded for the low- or high-density configurations, the maximum shoreward wave-induced force on the wall was consistently reduced for all wave cases considered.

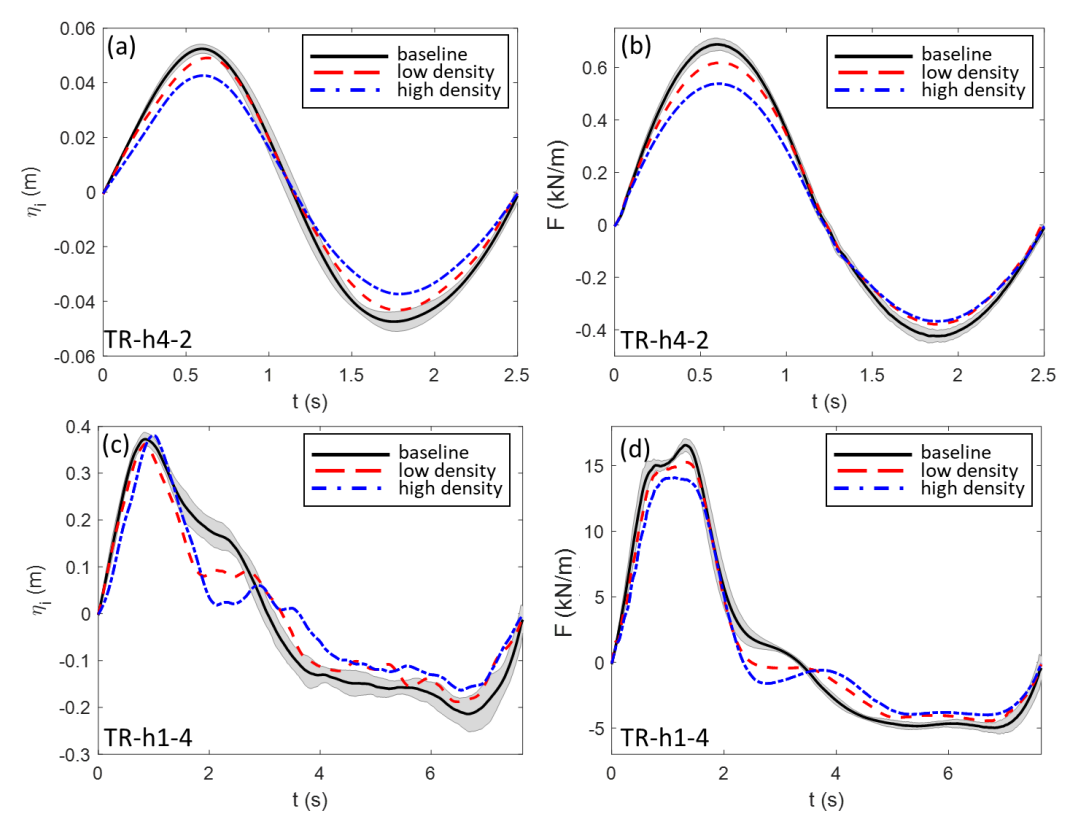


**Figure 8**: Ensemble average of free surface (a), (c) and force (b), (d) time series for baseline (black) with 95% confidence intervals (grey shading), low- (red dashed), and high-density (blue dash-dot curve) configurations for same conditions as Fig. 7.

For random waves, the incident and reflected free surface time series were separated using *Wavelab 3* (Frigaard and Lykke Andersen 2014) through a similar procedure as for regular wave cases (Zelt and Skielbreia 1992, Andersen et al. 2017, Gronbech et al. 1997). Pressure gauge time series were integrated vertically using trapezoidal rule to determine the instantaneous force time series on the wall. Representative incident wave parameters (wave heights and periods) were determined in the time domain based on zero-upcrossing analysis and in the frequency domain using a fast Fourier transformation of the water surface elevation time series. Several representative wave heights were computed. In the time domain, significant wave height (*i.e.*, the average of the highest one third of wave heights)  $H_{1/3}$ , average of the highest 10% of wave heights  $H_{1/100}$  were determined along

with the corresponding wave periods  $T_{I/3}$ ,  $T_{I/10}$ , and  $T_{I/100}$ . In the frequency domain, the spectral significant wave height  $H_{m0}$  and peak wave period  $T_p$  were calculated.

A similar procedure to that performed for time-domain water surface elevation analysis
was applied to the time series of integrated pressures (forces) to compute the mean wave force
$F_{mean}$ , and averages of the highest one third, 10%, 1%, and 0.4% of shoreward wave forces $F_{1/3+}$ ,
$F_{1/10+}$ , $F_{1/100+}$ , and $F_{1/250+}$ , respectively, as well as the corresponding negative 0.4%
representative force $F_{1/250}$ . Figure 9 presents examples of (a) incident water surface elevations
and (b) corresponding forces for 60 seconds for wave case TI-h2-1, with baseline incident
significant wave height $H_{m\theta} = 0.486$ m and peak period $T_p = 6.67$ s at Array 2 for the baseline
(black), low- (red dashed), and high-density (blue dash-dot) configurations. Figure 9 indicates
that the mangroves caused a time lag in the occurrence of water surface elevations at Array 2 and
forces on the wall, with the time lag increasing with forest density compared to the baseline
configuration. Additionally, Fig. 9b shows that the forces on the wall were reduced as density
increased from the baseline to low- to high-density configurations for the time series shown here.
These results are consistent for other wave cases in Appendix Table B.2, which presents
measured representative incident wave and water level parameters at Array 2 including $h_v$ , $H_{1/3}$ ,
$H_{m0}$ , $T_{1/3}$ , $T_p$ , measured representative integrated pressures (forces) on the wall $F_{1/3+}$ , $F_{1/10+}$ ,
$F_{1/100+}$ , and $F_{1/250+}$ and $F_{1/250-}$ , and the elevations above the bed $z$ at which $F_{1/250+}$ and $F_{1/250-}$ were
applied for all configurations and wave cases tested, $z_{F1/250+}$ and $z_{F1/250-}$ , respectively.

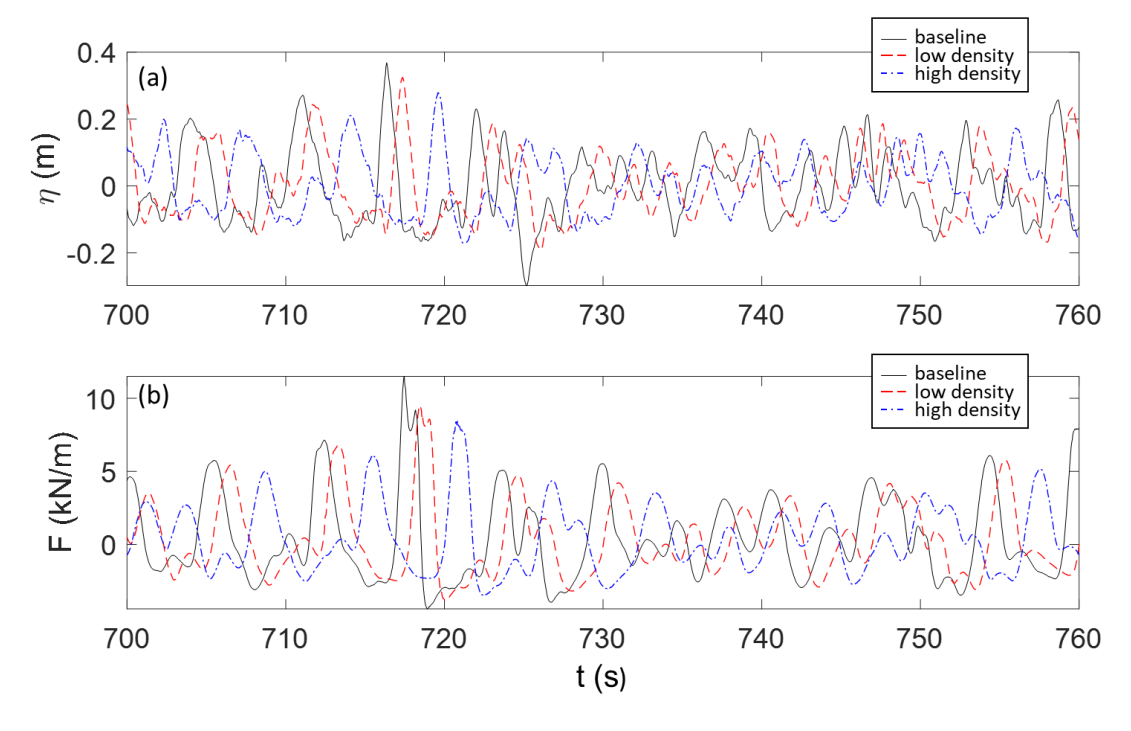


**Figure 9.** Detail of incident water surface elevation time series at Array 2 (a) and force per unit width (b) for wave case TI-h2-1 ( $h_v = 1.48 \text{ m}$ ,  $H_{m0} = 0.486 \text{ m}$  and  $T_p = 6.67 \text{ s}$ ) for baseline (black), low-density (red dashed), and high-density (blue dash-dot) configurations.

#### 2.3 Analytical Equations for Wave Force Estimation

The method presented by Goda (2010) was modified following Wiebe et al. (2014) and Tomiczek et al. (2019) to determine the pressure distribution on the vertical wall based on incident wave conditions. Parameters defining the pressure distribution are shown in Fig. 10.

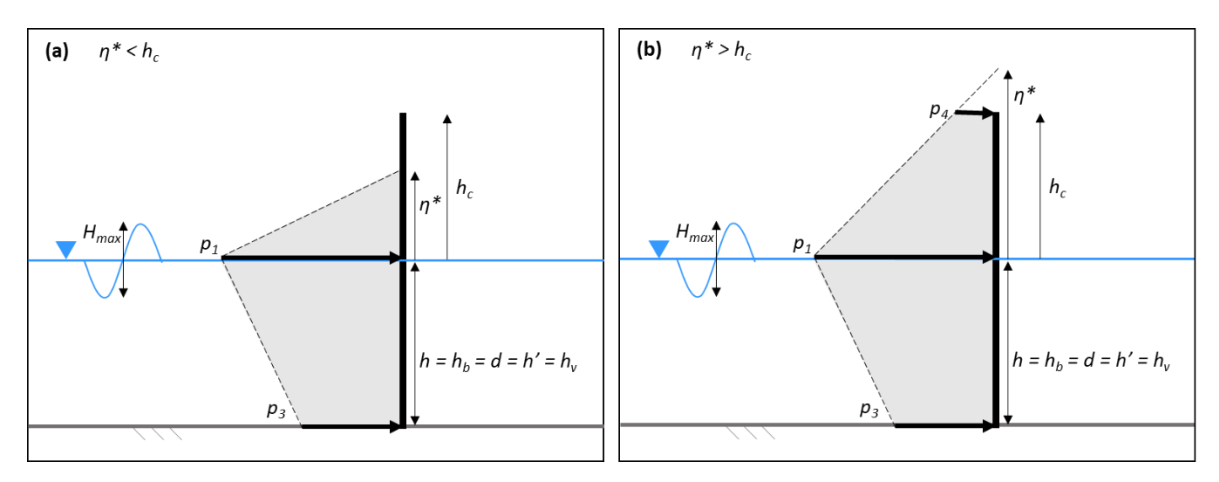


**Figure 10**. Wave-induced pressure distribution on a vertical wall and input variables for Goda (2010) equations for (a) elevation of zero wave pressure below wall crest elevation and (b) elevation of zero pressure above wall crest elevation.

As seen in Fig. 10, the maximum wave-induced pressure occurs at the still water line.

This pressure,  $p_1$ , was calculated as a function of the water density  $\rho$ , acceleration due to gravity, g, design wave height  $H_{max}$ , taken as 1.8 times the significant wave height, and geometry and

wave pressure coefficients as described in equation (1):

$$p_1 = \frac{1}{2}(1 + \cos\beta)(\alpha_1\lambda_1 + \alpha_2\lambda_2\cos^2\beta)\rho g H_{max}$$
 (1).

For these experiments, the angle of wave approach,  $\beta$ , was taken as  $0^{\circ}$  (*i.e.*, normal to the wall) and geometry coefficients  $\lambda_1$  and  $\lambda_2$  were set equal to 1. Wave pressure coefficients  $\alpha_1$  and  $\alpha_2$  are described in equations (2) and (3), respectively:

397 
$$\alpha_1 = 0.6 + \frac{1}{2} \left[ \frac{4\pi h/L}{\sinh{(4\pi h/L)}} \right]^2$$
 (2);

398 
$$\alpha_2 = \min\left\{\frac{h_b - d}{3h_b} \left(\frac{H_{max}}{d}\right)^2, \frac{2d}{H_{max}}\right\}$$
 (3),

where L is the wavelength and h, d, and  $h_b$  indicate water depths defined by Goda (2010) for a caisson breakwater elevated on a rubble mound; in the absence of a rubble mound and for a horizontal bottom as in these experiments, these parameters were equal and taken as the water depth at the vegetation  $h_v$ .

Goda (2010) defined the elevation above the still water level at which wave-induced pressure was zero,  $\eta^*$  as

405 
$$\eta^* = 0.75 (1 + \lambda_1 \cos \beta) H_{max}$$
 (4),

which simplified to  $\eta^* = 1.5 H_{max}$  for these tests. Pressure was assumed to vary linearly between  $p_1$  and  $\eta^*$ . Therefore, the pressure distribution on the portion of the wall above the still water level was either a triangle ( $\eta^* < h_c$ , Fig. 10a) with height  $\eta^*$  or a trapezoid ( $\eta^* > h_c$ , Fig. 10(b)) with pressure  $p_4$  at elevation equal to the crest height of the wall  $h_c$  found by linearly interpolating between  $p_1$  and  $\eta^*$ :

411 
$$p_4 = p_1 \left( 1 - \frac{h_c}{\eta^*} \right), \qquad \eta^* > h_c$$
 (5).

Below the still water level, pressure was assumed to vary linearly between  $p_1$  and the pressure at the bottom of the wall  $p_3$  as described in equation (6):

414 
$$p_3 = \left[1 - \frac{h'}{h} \left[1 - \frac{1}{\cosh(2\pi h/L)}\right]\right] p_1 \tag{6}$$

where h' defined by Goda (2010) can be taken as  $h_v$  in the absence of a rubble mound.

Using measured wave conditions at Array 2 shoreward of the mangrove forest,  $p_1$ ,  $p_3$ ,  $\eta^*$ , and  $p_4$  (where necessary) were calculated and integrated to estimate the force per unit width on the wall. For regular waves, we considered  $H_{max} = \overline{H}$  measured during experiments, and for random waves, we followed the recommendations of Goda (2010) taking the design wave height  $H_{max}$  equal to 1.8 times the measured incident significant wave height  $H_{m0}$ . These calculated forces were compared with measured forces obtained from integrating the pressure gauge time series on the wall.

#### 3. Wave Height and Force Observations and Effect of Mangroves

#### 3.1 Regular Wave Observations

Appendix Table B.1 presents the ensemble average maximum positive and negative wave-induced forces per unit width and their corresponding standard deviations for all regular wave cases. Ratios between the measured positive or negative force for the mangrove configurations to the corresponding positive or negative force for the baseline configuration,  $\overline{F_{+,N}}/\overline{F_{+,BL}}$  or  $\overline{F_{-,N}}/\overline{F_{-,BL}}$ , respectively, where N denotes either the HD or LD configuration are also presented in the table. Mangrove configurations reduced the positive force compared to the baseline configuration for all trials considered during experiments; as indicated in Appendix Table B.1, the high-density forest reduced shoreward (positive) forces compared to the baseline condition by 14% to 38%, while the low-density forest reduced positive forces compared to the baseline by 2% to 25%. The ratios of positive forces were generally greater at the higher two water depths tested (ranging 0.78 to 0.86 for the HD configuration and 0.84 to 0.98 for the LD configuration), compared to those computed at the lower two water depths (ranging 0.62 to 0.84 for the HD configuration and 0.75 to 0.91 for the LD configuration), suggesting that the greater projected areas of the lower two water depths reduced forces more significantly than conditions

with lower projected areas. These results are consistent with those of Kelty et al. (2022), who observed greater wave height attenuation for greater projected areas, as well as analytical formulations for wave height attenuation through vegetation (*e.g.*, Dalyrymple et al. 1984, Mendez and Losada 2004).

The high-density forest amplified seaward (negative) forces for three trials (TR-h2-5, TR-h3-5, and TR-h3-7), with amplification ranging between 11% to 17%, while the low-density forest amplified forces for one trial (TR-h2-5) by 13% compared to the baseline configuration. TR-h2-5 was one of the two trials in which wave height amplification was observed behind the mangrove forest for both configurations, which could have contributed to the amplified seaward force. For the majority of wave cases, mangroves reduced the seaward forces on the baseline configuration by up to 37% and 20% for the HD and LD configurations, respectively.

Figure 11 illustrates the effects of wave height and amount of attenuation on the maximum force per unit width. In the figure, the ensemble average maximum wave-induced force is plotted against the ensemble average incident wave height measured at Array 2, with symbols indicating the baseline (asterisks), low- (open circles), and high-density (filled circles) configurations and colors indicating water depths  $h_v = 1.85$  m (teal), 1.48 m (orange), 1.03 m (blue), and 0.73 m (black). Horizontal and vertical lines indicate 95% confidence intervals for wave heights and maximum forces, respectively. Conditions during which wave breaking was observed generally resulted in larger variation in measured wave height and force compared to non-breaking wave conditions. As seen in Fig. 11, as wave height increased, the measured force on the vertical wall also increased, consistent with relationships presented by Goda (2010) and Cuomo et al. (2010). However, consideration of unique wave conditions (observed in the figure as groupings of three points of the same color, with symbols for each configuration) indicates

that increasing the mangrove forest density tended to decrease both the wave height on the shoreward side of the forest as well as the resulting wave-induced force per unit width on the wall.

The ratio of the ensemble average minimum (seaward) force per unit width,  $\overline{F_-}$ , to the average maximum (onshore) force per unit width,  $\overline{F_+}$ , is presented for each wave condition in Appendix Table B.1. As indicated in the table, this ratio ( $\overline{F_-}/\overline{F_+}$ ) ranged between 0.14 and 1.04, indicating that for some wave conditions, the negative, seaward force exerted by the wave on the wall was of a similar order of magnitude or larger than the maximum positive, onshore force. Wave cases for which this ratio was greater than 0.9 had periods ranging between 1.57 s to 2.52 s and wave heights ranging between 0.122 m and 0.772 m. Comparison of the minimum to maximum force ratio between the BL, LD, and HD configurations indicated consistency across configurations for each unique wave condition. This result suggests that while the presence of mangroves reduced both the onshore and seaward forces on the wall, the processes associated with wave structure interaction were not affected.

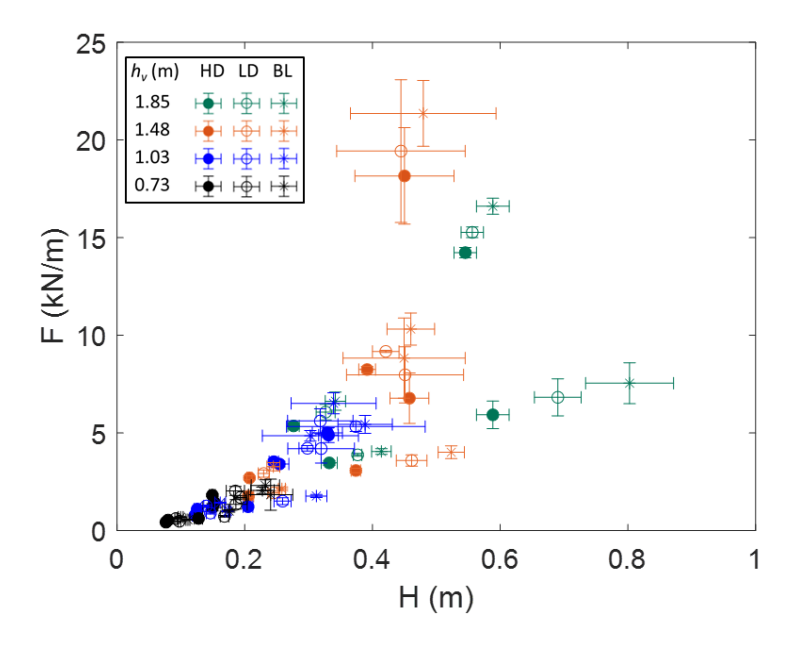


**Figure 11:** Measured peak shoreward wave force per unit width (kN/m) vs. incident wave height (m) at Array 2 for the BL (asterisks), LD (open circles), and HD (closed circles) configurations. Horizontal and vertical lines indicate 95% confidence intervals for wave height and force, respectively.

The pressure distribution at the time of the maximum and minimum forces for each wave condition and mangrove configuration was plotted to investigate effects of the vegetation on wave-induced pressures. Examples are provided in Fig. 12, which shows elevation above the bed z against corresponding maximum and minimum pressure measurements at the respective elevation, with 95% confidence intervals. Pressures measured at the time of the maximum (positive) force are shown as red symbols, and those measured at the time of the minimum (negative) force are shown as blue symbols. Color gradients indicate the baseline (light shades), low- (intermediate shades), and high-density (dark shades) configurations. The black vertical line in the center of each panel indicates the wall, and the blue horizontal line indicates the still water level for each trial. Measured pressure distributions were compared with the predicted pressure distribution computed using the method of Goda (2010), which is shown as dashed black lines in Fig. 12.

As seen in Fig. 12, the pressures recorded at each elevation tended to decrease from the baseline to low- to high-density configurations, resulting in the reduction in force observed in Fig. 11. Larger positive (onshore) wave forces are observed, although for some cases the negative (seaward) pressures were of a similar order of magnitude as the onshore pressures (Fig. 12a), consistent with the ratios  $(\overline{F_-}/\overline{F_+})$  presented in Appendix Table B.1 The shape of the pressure distribution was not affected by the presence or increased density of mangroves. Generally, the shape of the pressure distribution was consistent among the baseline, low-, and high-density configurations, particularly for non-impulsive wave conditions, and showed excellent agreement with predicted pressures from Goda (2010) (Fig. 12a,c). Breaking wave conditions (e.g., Fig. 12b) tended to generate larger peak forces, and greater variation was observed in measured positive pressures and the shape of the pressure distribution above the still water level, where impulsive wave breaking pressures may be expected. Likewise, the Goda (2010) method, which is intended for non-impulsive wave conditions, underestimated measured pressures. However, higher sampling rates are required in order to sufficiently capture these impulsive wave pressures. For a given wave condition, the location of the resultant force presented in Appendix Table B.1 is generally consistent across the baseline, low-density, and high-density mangrove configurations. This consistency in pressure distribution suggests that the fundamental processes associated with wave-structure interaction are unchanged by the presence of mangroves seaward of a structure of interest. Therefore, analytical methods for predicting the wave-induced pressures on a vertical structure such as that proposed by Goda (2010) may still be relevant considering pressures on a sheltered structure from transmitted waves through a mangrove forest.

517

495

496

497

498

499

500

501

502

503

504

505

506

507

508

509

510

511

512

513

514

515

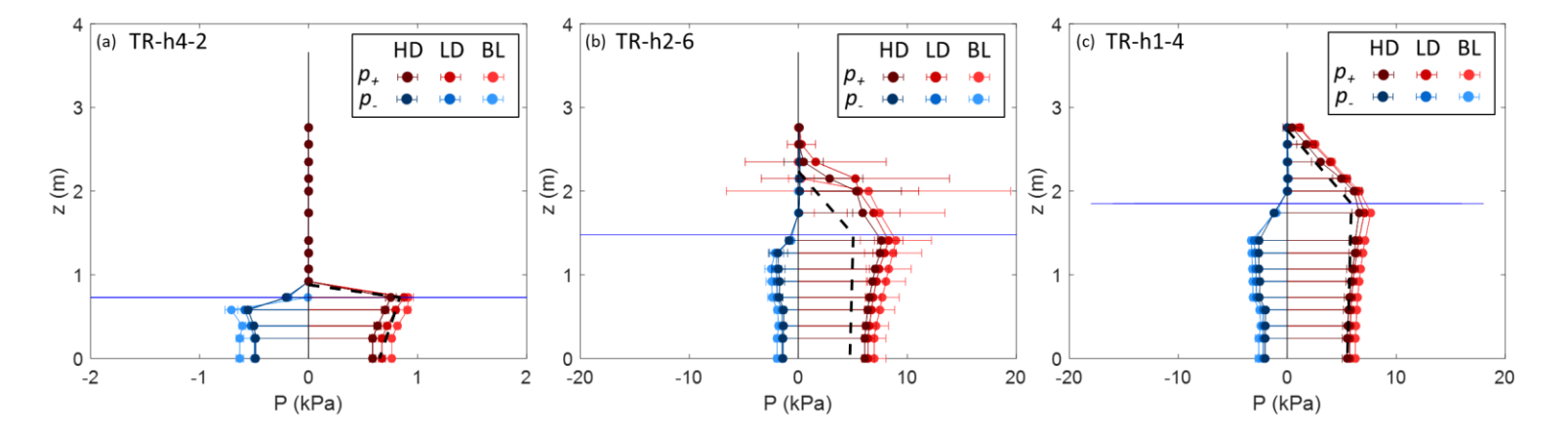


**Figure 12:** Example ensemble average pressure distributions with 95% confidence intervals at the time of the peak positive and negative forces; positive pressures  $p_+$  (red circles and lines) and negative pressures  $p_-$  (blue circles and lines) for the BL (light), LD (intermediate), and HD (dark) configurations. Black dashed lines indicate pressure distribution obtained from Goda (2010) using wave conditions measured at Array 2 for the BL configuration. Panels show wave conditions (a) TR-h4-2; (b) TR-h2-6; (c) TR-h1-4. Note difference in x-axis scale.

#### 3.2 Random Wave Observations

Appendix Table B.2 indicates wave heights and characteristic forces were consistently reduced from the baseline to the low- to the high-density configuration. Similar to Appendix Table B.1, ratios of the characteristic positive or negative forces measured during either the HD or LD mangrove configuration to those forces measured during the BL configuration are presented considering the  $1/250^{th}$  characteristic shoreward (positive) or seaward (negative) force. As shown in the table, the force ratio for the HD mangrove forest compared to the BL configuration ranged between 0.57 and 0.82 for positive forces and between 0.66 and 0.91 for negative forces, indicating reductions of 18 - 43% and 9 - 34% for positive and negative forces, respectively. The LD forest effected less of a force reduction than the HD forest, with positive forces reduced by 4 - 26% and negative forces reduced by 2 - 26% compared to the BL configuration. In contrast to regular wave conditions, no amplification was observed in seaward forces for any of the mangrove configurations or wave conditions tested.

Similar to the regular wave analysis, we considered the effects of wave parameters and mangrove configuration on measured wave forces. Fig. 13 shows the measured onshore and seaward  $1/250^{th}$  characteristic wave forces,  $F_{1/250+}$  and  $F_{1/250-}$ , respectively, plotted against the spectral significant wave height  $H_{m0}$  at Array 2. Symbols indicate the baseline (asterisks), low-(hollow circles), and high-density (filled circles) configurations, and colors indicate the water depth at the vegetation  $h_v = 1.85$  m (teal), 1.48 m (orange), 1.03 m (blue), and 0.73 m (black). Figure 13 indicates that for a given incident random wave condition, mangroves attenuated the wave heights, leading to a reduction in the magnitude of both  $F_{1/250+}$  and  $F_{1/250-}$ . Negative forces are nearly equal to or exceed positive forces for several wave cases, generally corresponding to measured wave forces less than approximately 5 kN/m. For larger wave forces, negative forces are less than positive forces by a factor of approximately two to three, yet are still of a similar

order of magnitude to the onshore-directed waves. As indicated in Appendix Table B.2, the wave period was not significantly affected by the presence of the low- or high-density mangrove forest.

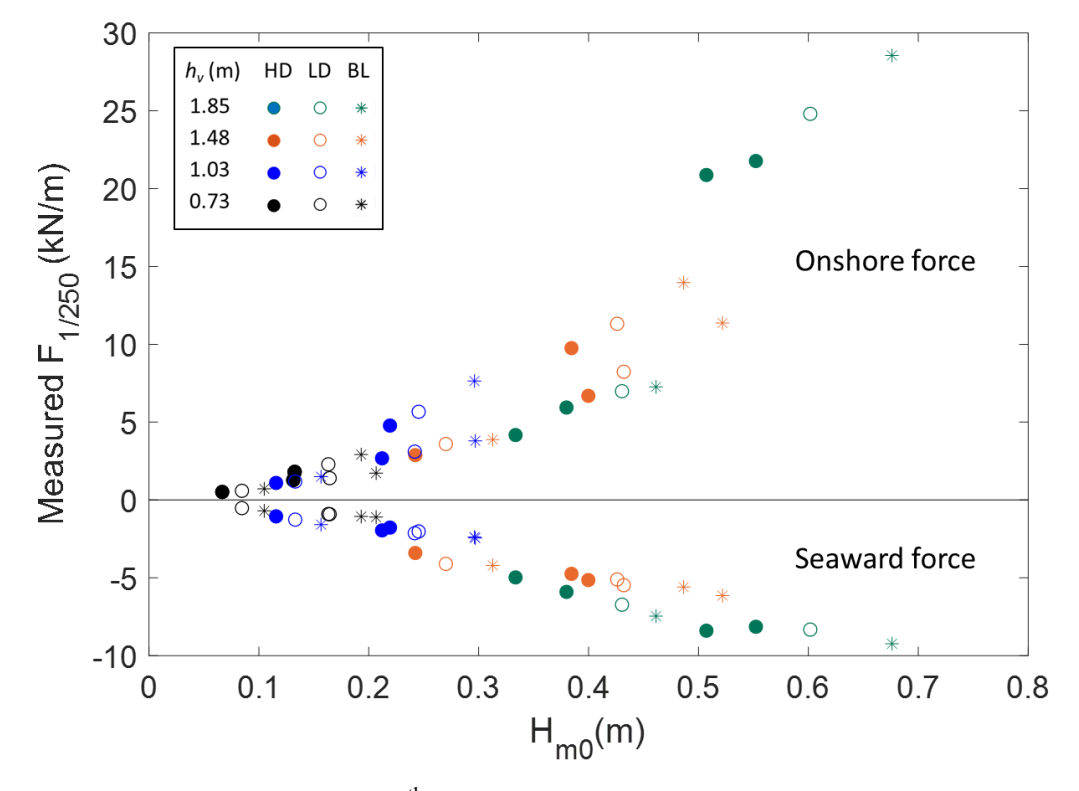


**Figure 13:** Measured top 1/250<sup>th</sup> of onshore (positive) and seaward (negative) forces per unit width (kN/m) versus measured significant wave height (m) at Array 2 for irregular wave conditions.

The pressure distributions at the time of the maximum and minimum forces were also determined for each wave case and specimen configuration; examples from three different wave cases are shown in Fig. 14, while the location of the resultant forces for all trials are presented in Appendix Table B.2. Similar to Fig. 12 for regular waves, blue colors in Fig. 14 indicate negative pressures and red colors indicate positive pressures for the baseline (light shades), low-(intermediate shades), and high-density (dark shades) configurations. Dashed lines denote the

pressure distribution predicted using the method of Goda (2010). Pressures associated with both the maximum (shoreward) and minimum (seaward) horizontal forces tended to decrease from the BL to LD to HD configurations. While some variability is observed (Fig. 14c), the shape of the pressure distribution and location of the resultant force  $F_{1/250+}$  or  $F_{1/250-}$  were generally constant for configurations with and without mangroves. Pressure distributions predicted by Goda (2010) were conservative and followed similar trends to measured pressures, although high pressures above the still water line were underestimated in Fig. 14c. This general agreement suggests that existing methods (*e.g.*, Goda, 2010) may be applied to determine the wave-induced force on a vertical wall, provided that accurate incident parameters are considered in the equations.

As seen in Fig. 14, the pressures associated with the minimum (negative) force are of a similar order of magnitude to those associated with the maximum (positive) force. Appendix Table B.2 similarly presents the ratio of the seaward top  $1/250^{th}$  wave force  $F_{1/250}$ - to the onshore top  $1/250^{th}$  wave force  $F_{1/250+}$  (*i.e.*,  $F_{1/250-}$  /  $F_{1/250+}$ ), which, for random wave trials, ranged between 0.31 and 1.19. Little variation in this ratio was observed for individual wave trials across the BL, LD, or HD configuration, indicating that the wave-structure interaction processes were not significantly affected by the presence or absence of a mangrove forest, beyond attenuation associated with reduced wave heights.

For several wave trials, the ratio of  $F_{1/250^-}$  /  $F_{1/250^+}$  was near or greater than one, indicating that seaward horizontal forces were nearly equal or greater than shoreward horizontal forces; wave conditions resulting in ratio values greater than 0.88 had spectral significant wave heights ranging between 0.067 m and 0.461 m and periods ranging between 1.67 s and 2.78 s. These conditions generally corresponded with smaller measured forces (less than approximately 5 kN/m). For larger measured forces, the negative forces were still significant compared to

# Manuscript to be summited to Nature-Based Solutions or Ocean Engineering

positive forces, generally less than onshore forces by a factor of approximately two to three.
These significant negative (seaward) pressures and forces were measured during experiments
across all configurations, including the baseline cases in which mangroves were not present.
These observations suggest that these seaward pressures and forces may be a possible
mechanism contributing to the seaward failure of seawalls during storms and should be
considered in design of vertical walls impacted by waves.



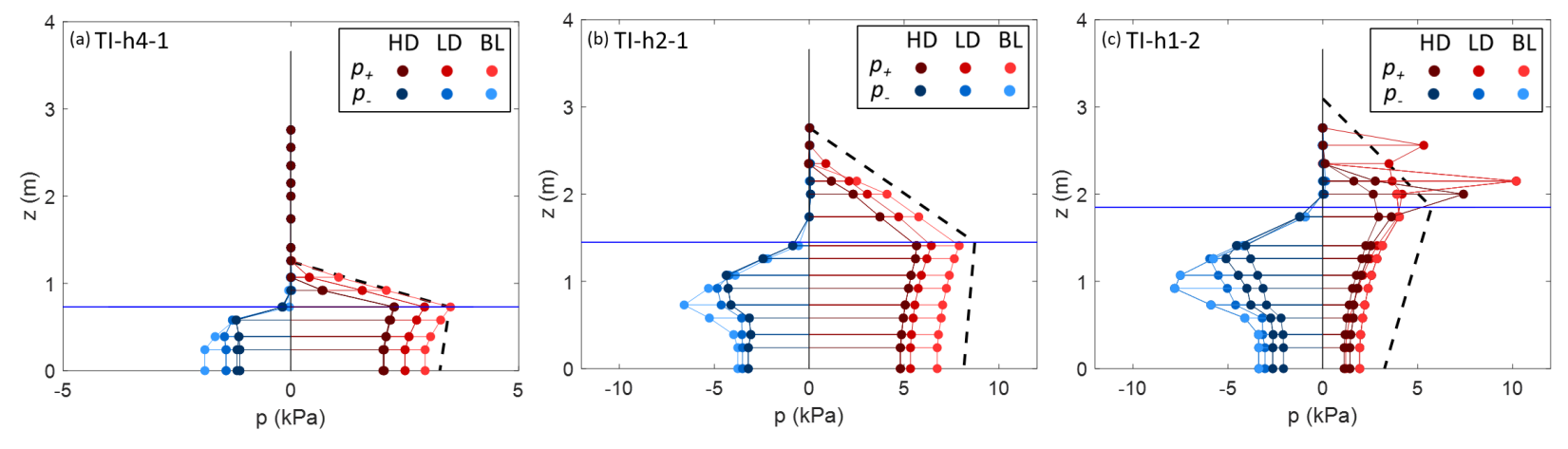


**Figure 14:** Example pressure distributions at the time of the maximum positive (red circles and lines) and negative (blue circles and lines) for the BL (light), LD (intermediate), and HD (dark) configurations. Black dashed lines indicate pressure distribution obtained from Goda (2010) using wave conditions measured at Array 2 for the BL configuration. Panels show wave conditions (a) TI-h4-1; (b) TI-h2-1; (c) TI-h1-2. Note difference in *x*-axis scale.

#### 3.3 Comparison with Existing Formulations

Observations for regular and random waves suggest that for the wave conditions tested, the presence of mangroves served to reduce the wave height interacting with the wall compared to the baseline condition, thus reducing the total force without significantly changing the shape of the pressure distribution or other processes associated with wave structure interaction.

Therefore, we investigated the ability of the semi-empirical method proposed by Goda (1974, 2010) to predict the wave-induced force using the attenuated wave height as input.

Figure 15 shows the measured ensemble average force for all regular wave trials plotted against the force calculated using Goda (2010), applying the measured wave height and period at Array 2 as inputs and assuming  $H_{max} = \overline{H}$ . Symbols indicate the baseline (asterisks), low- (open circles), and high-density (closed circles) configurations and are colored by the measured wave height at Array 2. In general, the semi-empirical equations accurately predict the measured wave force independent of configuration. The average percent difference between measured and predicted forces is 10%. For case TR-h2-6 with  $h_v = 1.48$  m,  $\overline{H} = 0.503$  m,  $\overline{T} = 6.90$  s for the BL configuration, measured forces are 60% greater than predicted; we note that impulsive wave breaking was observed for these conditions, while the method of Goda (2010) is not intended for waves that break directly on the structure. In such instances, other formulae should be considered (e.g., Minikin 1963, Cuomo et al. 2010).

Similar to Fig. 15, Fig. 16 shows the comparison of measured top  $1/250^{th}$  wave forces with those forces predicted using Goda (2010) for random wave conditions, applying the measured significant wave heights and peak periods at Array 2 and taking  $H_{max} = 1.8H_{m0}$  in the calculation of the wave-induced pressure distribution. In general, predicted forces generally agree with measurements and are not affected by the test configuration. In contrast with regular wave results, predicted forces are generally conservative compared to measured values, which

may partially stem from considering the maximum wave height in the sea state as recommended by Goda (2010). These results suggest that given accurate information about wave characteristics, the method of Goda (2010) can be used for conservative estimates of the wave force on a vertical wall. Thus, the load reduction on a sheltered structure due to mangroves may be determined if wave height attenuation through the vegetation is accurately incorporated into existing semi-empirical equations.

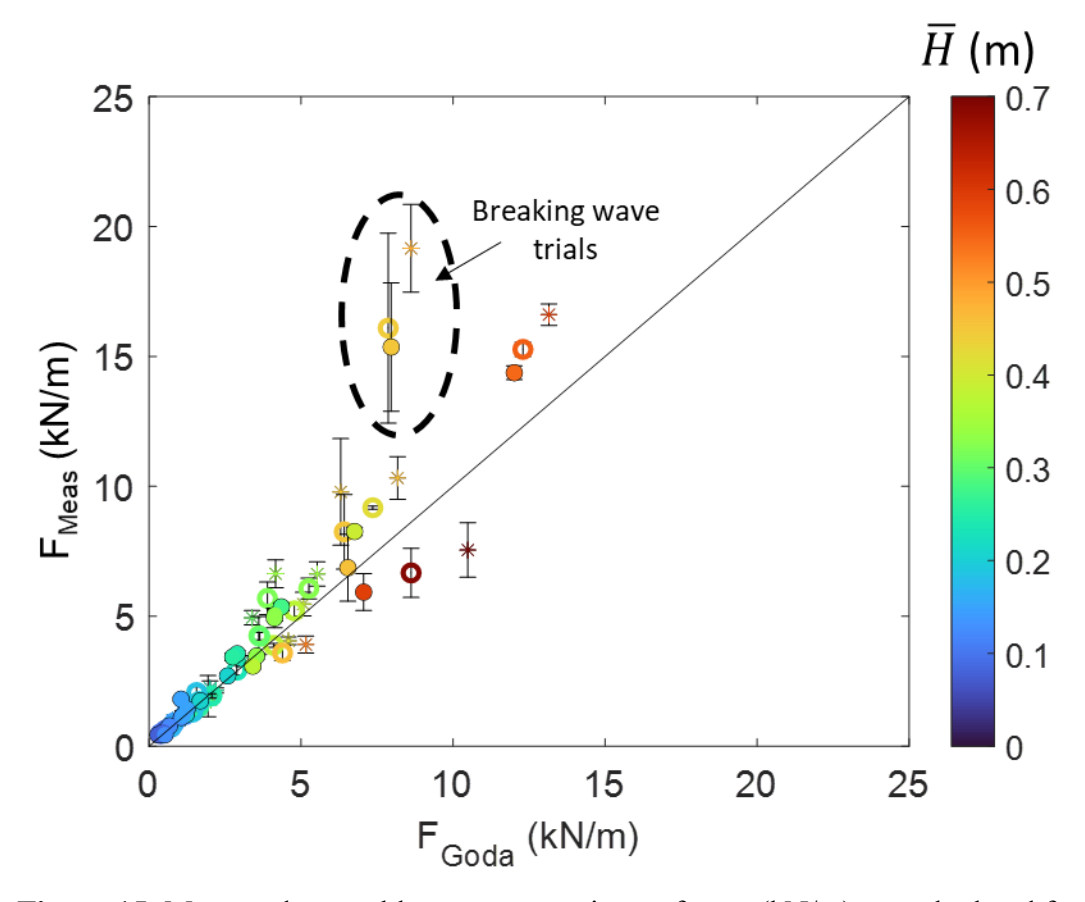


**Figure 15**: Measured ensemble average maximum forces (kN/m) vs. calculated forces using the Goda (2010) model for regular wave conditions. Symbols indicate baseline (asterisks), LD (open circles), and HD (closed circles) configurations and are colored by measured ensemble average wave height at Array 2. Black line indicates 1:1 agreement, and error bars indicate 95% confidence intervals in measured forces.

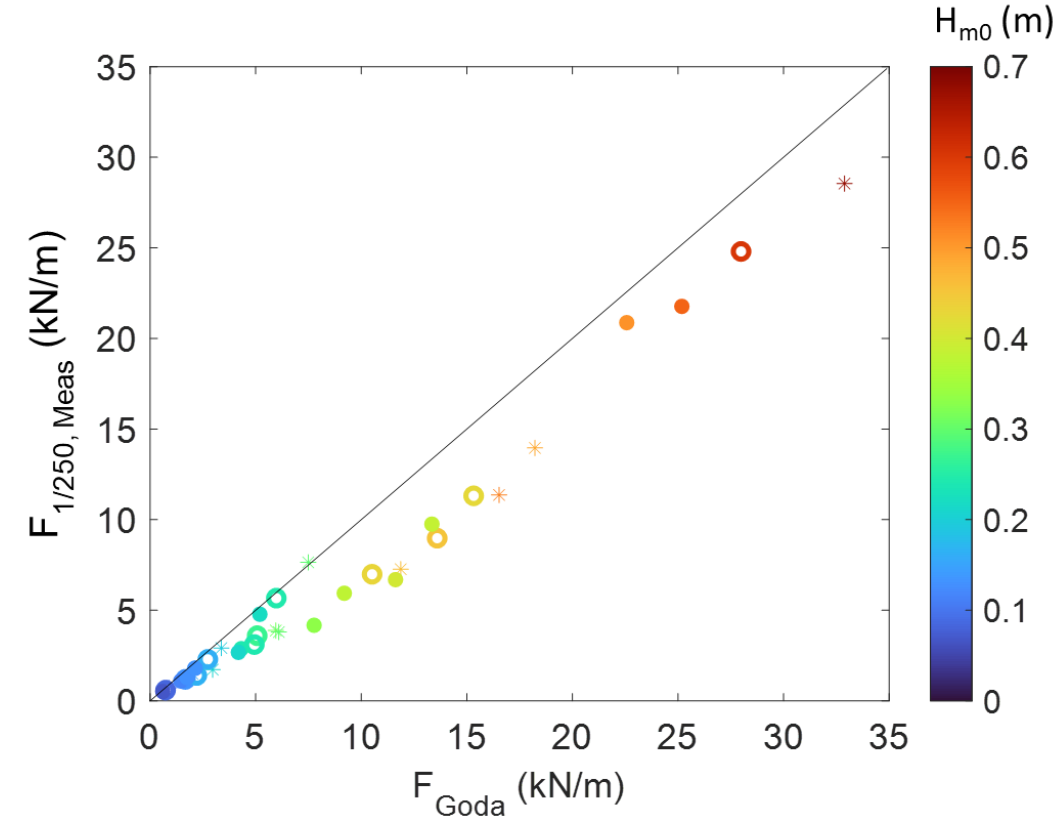


**Figure 16**: Measured top 1/250<sup>th</sup> shoreward force (kN/m) vs. calculated force using the Goda (2010) model for random wave conditions. Symbols indicate baseline (asterisks), LD (open circles), and HD (closed circles) configurations and are colored by measured spectral significant wave height at Array 2. Black line indicates 1:1 agreement.

### 4. Discussion

While wave height attenuation through mangrove forests of moderate cross-shore widths has been well documented, the effects of that wave height attenuation on performance metrics such as the reduction in wave force, runup, overtopping and erosion are not as well understood. This study is the first prototype-scale, quantitative investigation of both wave height reduction through an idealized mangrove forest and the resulting reduction in the wave-induced force on a sheltered vertical wall. At a 1:1 geometric scale, these experiments provide information on wave-vegetation-structure interaction in the absence of scale effects and can be used in future studies evaluating scale effects to more confidently interpret results of reduced-scale studies. Wave

heights generally decreased with increasing forest density, although for two regular wave trials (TR-h2-5 and TR-h3-5), the ensemble average wave height behind the mangrove forest decreased insignificantly (by <2%) or increased compared to the BL configuration. This increase in wave height was likely due to wave breaking seaward of the mangrove forest; even in these conditions, the presence of mangroves caused a reduction in the shoreward wave-induced force on the wall, although in few instances the seaward wave force was amplified.

Shoreward wave forces measured on the wall during the baseline configuration were consistently reduced by the HD or LD mangrove forest. Appendix Table B.2 shows that the low-density mangrove forest configuration caused wave force reductions ranging from 2% to 25% and 4% to 26% for regular and random waves, respectively, while the high-density forest configuration caused wave force reductions ranging from 14% to 38% and 18% to 43% for regular and random waves, respectively. These force reductions are significant, particularly considering the moderate cross-shore width (18 m) of the model forest, resulting in forest-to-wavelength ratios ranging between 0.56 and 5.39. The results of this experiment suggest that shoreward (positive) wave force decay rates of 0.1 – 1.4 %m<sup>-1</sup> for the low-density forest and 0.8 – 2.4 %m<sup>-1</sup> for the high-density forest. Longer forest widths may be expected to provide even greater protection for nearshore infrastructure.

As seen in Figs. 15 and 16, analytical equations proposed by Goda (1974, 2010) gave a reasonable estimate of the wave-induced force on a vertical wall, provided accurate information about incident wave conditions. These results have implications for incorporating mangroves or other vegetation into engineering design; with knowledge of wave height attenuation through a known distance of emergent vegetation, engineers can predict the expected wave load reduction on a sheltered structure. Future work may investigate the coupled performance of methods to

predict wave height attenuation (Dean and Dalrymple 1984, Mendez and Losada 2004) with force-prediction equations (Goda et al. 2010). Similarly, the expected reduction in damages to the built environment may be determined based on fragility relationships between wave load and structural capacity (Do et al. 2020). Quantifying the performance of mangrove systems may facilitate greater implementation of nature-based and hybrid infrastructure systems in future shore protection designs.

Across all configurations, negative (seaward) wave pressures and forces were nonnegligible, and for several wave conditions these loads were nearly equal or greater than the measured positive (onshore) wave pressures and forces (Appendix Tables B.1 and B.2). While the largest onshore wave forces measured were approximately two to three times larger than the seaward forces, these negative forces were still of a similar order of magnitude as the positive forces. Significant negative wave forces on armor units have been measured and can be a concern for the stability of offshore breakwaters (Boccotti et al. 2011, Douglas et al. 2020); likewise, measurements in these tests indicate that negative forces and pressures could contribute to the damage and failure of coastal or onshore infrastructure such as seawalls or vertical walls of near-coast structures. While robust guidance exists for predicting horizontal wave forces on vertical walls in the direction of wave propagation (e.g., ASCE 2022), little information is available for predicting negative loads associated with the wave trough. Results of these experiments suggest that seaward forces should be considered in the design of walls and other structural elements affected by waves.

While experimental measurements indicated load reduction by the mangrove forest, caution must be taken when interpreting results for application to real-world systems. The specimens considered here were idealizations of the *Rhizophora* mangrove using the model of

703

704

705

706

707

708

709

710

711

712

713

714

715

716

717

718

719

720

721

722

723

724

Ohira et al. (2013); other studies have likewise proposed parameterizations to the *Rhizophora* trunk-prop root system based on field surveys of mangrove specimens (Mori et al. 2022). While the model dimensions and forest densities were selected to be within ranges reported from field studies, greater variation is expected in a natural or restored mangrove system, both in the root structure and layout of individual trees. Further, the specimens tested in these experiments included only the trunk and prop root system of the Rhizophora specimens, and any effects of the mangrove canopies (branches and leaves) on wave height or wave force attenuation were not considered. Previous studies have reported that when submerged, mangrove canopies are important for wave height dissipation, and neglecting the canopy can lead to underestimation of wave height attenuation potential of the mangrove forest (Zhang et al. 2023). Future work may similarly consider the effect of mangrove branches and leaves in wave force reduction on sheltered structures. While the experiments presented in this work considered a mature mangrove forest, the lifecycle performance of the system must be considered for engineering design. This performance may vary temporally as a juvenile forest matures and changes due to in situ ecological and environmental parameters, or under in combination with other vegetation archetypes in heterogeneous forests. The vulnerability of a forest to damage or degradation due to acute and chronic hydrodynamic and biological stressors must also be considered.

For two wave cases conducted at the highest water depth, wave-induced pressures at the topmost gauge were nonzero, indicating forces on the wall between the highest gauge and wall crest. These pressures and forces may impact the stability of overtopped seawalls, and future studies may consider additional pressure gauges to more accurately determine pressures acting near the crest of an overtopped wall. In few trials, typically associated with wave breaking at the wall, variability in measured pressures increased at each elevation, and the elevation at which the

peak pressure occurred above the still water level and changed from the baseline to the low- and high-density configurations. These observations are consistent with observations by Tomiczek et al. (2019, 2020b). Pressures associated with breaking wave impact can be highly variable and are affected by the shape of the breaking wave and level of air entrainment (Chan and Melville 1988, Cooker and Peregrine 1990, Bredmose et al. 2015), and high impulsive pressures may be important when considering localized damage. For mangrove forests of moderate cross shore widths, these effects of the forest on the wave breaking characteristics and location of the peak pressure on a sheltered structure may become important, while forests of longer cross shore widths (*O*~1 km) may be expected to reduce wave heights such that breaking will eventually stop. Future studies conducted at higher sampling rates and under a wider variety of breaking wave conditions are needed to investigate the effects of mangrove forests of small or moderate cross shore widths on wave breaking processes and the resulting interaction with sheltered structures.

### 5. Conclusions

This paper presents results from a prototype-scale experiment measuring wave height transformation through an idealized mangrove forest of 18 m cross shore width and the resulting wave force reduction on a sheltered vertical wall. The research objectives of this experiment were to (1) evaluate the effectiveness of mangrove systems in mitigating wave-induced loads on sheltered structures, and (2) assess the ability of existing analytical methods for wave force prediction to determine wave forces on structures sheltered by mangrove forests, using the attenuated wave conditions as inputs. We considered 23 regular and 11 random wave cases at four water depths propagating through a baseline condition with no mangroves and two forest densities (0.75 stems/m² and 0.375 stems/m²). We compared measured pressure distributions

and forces with predicted values using the method of Goda (1974, 2010). These analyses draw four main conclusions:

- 1. As mangrove forest density increased, the wave pressures and forces on the vertical wall positioned shoreward of the forest section decreased due to the attenuation of waves through the mangrove trunk and prop root systems. Force reductions of 2% to 38% were observed for regular wave conditions, and the  $F_{1/250}$  force was reduced by 4% to 43% for random waves.
- 2. For nonbreaking wave trials, increasing the mangrove forest density tended to reduce measured pressures without changing the shape of the pressure distribution. This result suggests that the vegetation did not significantly change the wave-structure interaction processes for nonbreaking waves.
- 3. Existing equations for calculating nonbreaking wave forces (Goda 1974, 2010) showed very good agreement with measured forces when the measured wave conditions shoreward of the mangrove forest were used. The calculated forces slightly underpredicted the observed ensemble average forces in regular wave trials (*i.e.* were slightly non-conservative), and the calculated forces generally overpredicted (*i.e.* were conservative) in estimating the observed top 1/250<sup>th</sup> characteristic force for random wave conditions. This suggests that the expected reduction in wave force due to sheltering by mangroves can be estimated using existing equations when the wave attenuation is predicted accurately.
- 4. Negative (seaward) forces associated with the wave trough were equal to the positive (onshore) forces for smaller wave forces (less than approximately 5 kN/m) and approximately two to three times less than the largest onshore forces (Fig. 13). These

observations show that the offshore-directed forces, though smaller, are of similar magnitude to the onshore directed forces for large waves. More importantly, these offshore forces would contribute to the seaward destabilization of vertical seawalls observed after large storms and may need to be considered in the design of coastal infrastructure affected by waves.

As communities around the world search for climate resilient and climate-mitigating solutions with increasing urgency, nature-based solutions show promise for delivering blue-carbon benefits, ecological services, and coastal flood hazard mitigation. Increased understanding of the performance of these systems is vital to developing quantified, practical guidance to broaden the implementation of these systems.

### Acknowledgements

The authors gratefully acknowledge HWRL staff Tim Maddux, Rebekah Miller, and participating undergraduate students for testing assistance. Two anonymous reviewers provided helpful feedback on an earlier draft of this manuscript. This project was supported by funding from the National Science Foundation through CMMI awards 1661315, 1825080, and 2037914, and CBET awards 2110262 and 2110439, and from the U.S. Army Corps of Engineers through project number W912HZ2120045. Any opinions, findings, conclusions, or recommendations expressed in this material are those of the authors and do not necessarily reflect the views of the National Science Foundation, U.S. Army Corps of Engineers, or U.S. Naval Academy.

#### **Authorship Contribution Statement**

Tomiczek: Experimental design, supervision, visualization, writing original draft, review and editing; Mitchell: Conducting experiment, data analysis, visualization, writing original draft, review and editing; Lomónaco: Experimental design, supervision, visualization, writing original

- draft, review and editing; Cox: Experimental design, supervision, review and editing; Kelty:
- 795 Experimental design, conducting experiment, data analysis, review and editing.
- 796 References

- Andersen, T. L., Eldrup, M. R., & Frigaard, P. (2017). Estimation of incident and reflected components in
- highly nonlinear regular waves. *Coastal Engineering* (119) 51-64.
- 799 https://doi.org/10.1016/j.coastaleng.2016.08.013
- 800 ASCE. (2022). Minimum design loads and associated criteria for buildings and other structures.
- 801 ASCE/SEI 7-22. Reston, VA: ASCE. https://doi.org/10.1061/9780784415788
- Blackmore, P. A., and P. J. Hewson. (1984). Experiments on full-scale wave impact pressures. *Coastal Eng.* 8 (4): 331–346. https://doi.org/10.1016/0378-3839(84)90029-2.
- Boccotti, P., Arena, F., Fiamma, V., Romolo, A., and Barbaro, G. (2011). Small-scale field experiment on wave forces on upright breakwaters. *Journal of Waterway, Port, Coastal, and Ocean Engineering*. 138 (2), 97-114. https://doi.org/10.1061/(ASCE)WW.1943-5460.0000111.
- Bredes, A., Miller, J.K., Kerr, L., Gannon, K., and Day, I. (2023). Developing guidance for the
  application of Natural and Nature Based Features (NNBF) on developed shores: A case study from
  New Jersey, USA. *Regional Studies in Marine Science*, 62 (2023) 102959.
  https://doi.org/10.1016/j.rsma.2023.102959
- Bredmose, H., G. N. Bullock, and A. J. Hogg. (2015). Violent breaking wave impacts. Part 3: Effects of scale and aeration. *J. Fluid Mech.* 765: 82–113. https://doi.org/10.1017/jfm.2014.692.
- Bridges, T. S., King, J. K., Simm, J. D., Beck, M. W., Collins, G., Lodder, Q., et al. (2021). International
   Guidelines on Natural and Nature-Based Features for Flood Risk Management. Engineer Research
   and Development Center (U.S.) <a href="https://hdl.handle.net/11681/41946">https://hdl.handle.net/11681/41946</a>.
- Bryant, M.A., Bryant, D.B., Provost, L.A., Hurst, N., McHugh, M., Wargula, A., Tomiczek T. (2022).
   Wave Attenuation of coastal mangroves at a near-prototype scale. USACE Engineer Research and
   Development Center, ERDC TR-22-17. Vicksburg, MS.
- Bullock, G.N., Obhrai, C., Peregrine, D.H., Bredmose, H., 2007. Violent breaking wave impacts. Part 1:
   results from large-scale regular wave tests on vertical and sloping walls. *Coast. Eng*, 54 (2007), 602–
- 823 617.
  824
  825 Castellari, S., Zandersen, M., Davis, M., Veerkamp, C., Förster, J., Marttunen, M., Mysiak, J.,
  826 Vandewalle, M., Medri, S., and Picatoste, J.R. (2021). *Nature-based solutions in Europe: policy*,
- knowledge and practice for climate change adaptation and disaster risk reduction. European
   Environment Agency, Publications Office https://doi.org/10.2800/919315.
- Chan, E. S., and Melville, W. K. (1988). Deep-water plunging wave pressures on a vertical plane wall, 830 *Proc. R. Soc. London.* A 417, 95-131. https://doi.org/10.1098/rspa.1988.0053
- 831 Chang, C.-W., Mori, N., Tsuruta, N., and Suzuki, K. (2019). Estimation of Wave Force Coefficients on
- Mangrove Models. J. Jpn. Soc. Civ. Eng. Ser B2 Coast. Eng.,
- https://doi.org/10.2208/kaigan.75.I 1105.

Chen, C., Peng, C., Nandasena, N.A.K. Yan, H., and Zhan, Z. (2023). Protective effect of ecological embankment on a building subjected to tsunami bores. *Ocean Engineering*, 280 (2023) 114638. https://doi.org/10.1016/j.oceaneng.2023.114638

- Cooker, M. J., and D. H. Peregrine. (1990). Computation of violent wave motion due to waves breaking against a wall. *In Proc.*, 22<sup>nd</sup> *Int. Conf. on Coastal Engineering*, edited by B. L. Edge, 164–167.
   Reston, VA:ASCE. ISBN 0-87262-776-4
- Cuomo, G., W. Allsop, T. Bruce, and J. Pearson. (2010). Breaking wave loads at vertical seawalls and breakwaters. *Coastal Engineering*, 57 (4): 424–439. https://doi.org/10.1016/j.coastaleng.2009. 11.005.
- Dalrymple, R.A., Kirby, J.T., Hwang, P.A. (1984). Wave Diffraction Due to Areas of Energy Dissipation.
   Journal of Waterway, Port, Coastal, and Ocean Engineering 110, 67–79.
   <a href="https://doi.org/10.1061/(ASCE)0733-950X(1984)110:1(67)">https://doi.org/10.1061/(ASCE)0733-950X(1984)110:1(67)</a>
  - Danielsen, F., Sørenson, M.K., Olwig, M.F., Selvam, V., Parish, F., Burgess, N.D., Hiraishi, T., Karunagaran, V.M., Rasmussen, M.S., Hansen, L.B., Quarto, A., Suryadiputra, N., (2005). The Asian Tsunami: A protective role for coastal vegetation. *Science* 310 (5748), 643. <a href="https://doi.org/10.1126/science.1118">https://doi.org/10.1126/science.1118</a>
- Dawes, C., Siar, K., and Marlett, D. (1999). Mangrove structure, litter and macroalgal productivity in a Northern-most forest of Florida. *Mangroves Salt Marshes* 3, 259–267. doi: 10.1023/A:1009976025000
  - Do, T., van de Lindt, J.W., and Cox, D.T. (2020). Hurricane Surge-Wave Building Fragility Methodology for Use in Damage, Loss, and Resilience Analysis. *J. Structural Engineering*, 146 (1) https://doi.org/10.1061/(ASCE)ST.1943-541X.0002472.
  - Douglas, S., Cornett, A., and Nistor, I. (2020). Image-based measurement of wave interactions with rubble mound breakwaters. *J. Mar. Sci. Eng.* 2020 8 (6), 472. https://doi.org/10.3390/jmse8060472
  - Faivre, N., Fritz, M., Freitas, T., de Boissezon, B., and Vandewoestijne, S. (2017). Nature-based solutions in the EU: Innovating with nature to address social, economic, and environmental challenges. *Environmental Research*, 159 (2017) 509-518. https://doi.org/10.1016/j.envres.2017.08.032
  - Fathi-Moghadam, M., Davoudi, L., and Motamedi-Nezhad, A. (2018). Modeling of solitary breaking wave force absorption by coastal trees. *Ocean Engineering*, 169 (2018) 87-98. https://doi.org/10.1016/j.oceaneng.2018.09.021
  - Frigaard, P. and Lykke Andersen, T. (2014). *Analysis of Waves. Technical documentation for WaveLab 3*. DCE Lecture Notes No. 33, Aalborg University, Denmark
- Goda K., N. Mori, T. Yasuda, A. Prasetyo, A. Muhammad, and D. Tsujio. (2019). Cascading Geological
   Hazards and Risks of the 2018 Sulawesi Indonesia Earthquake and Sensitivity Analysis of Tsunami
   Inundation Simulations. Front. Earth Sci. 7:261. https://doi.org/10.3389/feart.2019.0
- Goda, Y. (1974). New wave pressure formulae for composite breakwaters. *Proceedings of the 14<sup>th</sup> International Coastal Engineering Conference*, Vol 3, pp. 1702-1720.

884 Goda, Y. (2010). Random Seas and Design of Maritime Structures. 3rd ed. World Scientific 885 https://doi.org/ 10.1142/7425. 886 887 Gronbech, J., Jensen, T., & Andersen, H. (1997). Reflection Analysis with Separation of Cross Modes. 888 *Proceedings of the Coastal Engineering Conference*, 1, (pp. 968-980). 889 https://doi.org/10.1061/9780784402429.076 890 891 Guannel, G., K. Arkema, P. Ruggiero, and G. Verutes. (2016). The Power of Three: Coral Reefs, 892 Seagrasses and Mangroves Protect Coastal Regions and Increase Their Resilience. PLoSONE 11(7) 893 https://doi.org/10.1371/journal.pone.0158094 894 895 Hardaway, Jr., C.S., Milligan, D.A., Duhring, K., & Wilcox, C.A. (2017). Living shoreline design 896 guidelines for shore protection in Virginia's estuarine environment (SRAMSOE #463). Gloucester 897 Point, VA: Virginia Institute of Marine Science. https://doi.org/10.21220/V5CF1N 898 899 Heidarzadeh, M., Teeuw, R., Day, S., and Solana, S. (2018). Storm wave runups and sea level variations 900 for the September 2017 Hurricane Maria along the coast of Dominica, eastern Caribbean Sea: 901 evidence from field surveys and sea-level data analysis. Coastal Engineering Journal, 60 (3), 371-902 384. https://doi.org/10.1080/21664250.2018.1546269 903 904 Horstman, E. M., C. M. Dohmen-Janssen, P. M. F. Narra, N. J. F. van den Berg, M. Siemerink, and S. J. 905 M. H. Hulscher. (2014). Wave Attenuation in Mangroves: A Quantitative Approach to Field 906 Observations. Coastal Engineering 94(2014): 47–62. https://doi.org/ 907 10.1016/j.coastaleng.2014.08.005 908 909 ICC (International Code Council). (2015). International building code. Washington, DC: ICC. 910 Jimenez, J. A., Lugo, A. E., and Cintron, G. (1985). Tree mortality in Mangrove Forests, Biotropica 911 17:177. https://doi.org/10.2307/2388214 912 Keimer, K., Schürenkamp, D., Miescke, F., Kosmalla, V., Lojek, O., Goseberg, N. (2021). Ecohydraulics 913 of Surrogate Salt Marshes for Coastal Protection: Wave-Vegetation Interaction and Related 914 Hydrodynamics on Vegetated Foreshores at Sea Dikes. Journal of Waterway, Port, Coastal, and Ocean Engineering 147 (6). https://doi.org/10.1061/(ASCE)WW.1943-5460.0000667 915 916 Kelty, K., Tomiczek, T., Cox, D., and Lomonaco, P. (2021). Prototype-scale physical model study of 917 wave attenuation by an idealized mangrove forest of moderate cross-shore width, in Experimental 918 Investigation of Wave, Surge, and Tsunami Transformation over Natural Shorelines, ed. DesignSafe, 919 https://doi.org/10.17603/ds2-znjw-1f81 920 Kelty, K., Tomiczek, T., Cox, D. T., Lomonaco, P., and Mitchell, W. (2022). Prototype-Scale Physical 921 Model of Wave Attenuation Through a Mangrove Forest of Moderate Cross-Shore Thickness: 922 LiDAR-Based Characterization and Reynolds Scaling for Engineering With Nature. Front. Mar. Sci. 8. doi: https://doi.org/10.3389/fmars.2021.780946. 923 924 Loría-Naranjo, M., Samper-Villarreal, J., and Cortés, J. (2014). Structural complexity and species 925 composition of Potrero Grande and Santa Elena Mangrove Forests in Santa Rosa National Park,

927 Marsh, G. (2024). LOESS regression smoothing,

926

928 (https://www.mathworks.com/matlabcentral/fileexchange/55407-loess-regression-smoothing),

North Pacific of Costa Rica. Rev. Biol. Trop. 62, 33–41. https://doi.org/10.15517/rbt.v62i4.20030

929 MATLAB Central File Exchange. Retrieved February 20, 2024.

- 930 Marsooli, R. and Lin, N. (2018). Numerical modeling of historical storm tides and waves and their
- interactions along the U.S. East and Gulf coasts. *JGR Oceans*. 123 (5), 3844-3874.
- 932 https://doi.org/10.1029/2017JC013434
- 933 *Matlab*. Version 2021b. Mathworks, 28 Sep. 2021.
- 934 Maza, M., J. L. Lara, and I. J. Losada. (2019). Experimental Analysis of Wave Attenuation and Drag
- Forces in a Realistic Fringe Rhizophora Mangrove Forest. *Advances in Water Resources* 131(2019):
- 936 1033. https://doi.org/10.1016/j.advwatres.2019.07.006
- 937 Maza, M., Lara, J. L., and Losada, I. J. (2021). Predicting the evolution of coastal protection service with
- 938 mangrove forest age. *Coast. Eng.* 168, 103922. https://doi.org/10.1016/j.coastaleng.2021.103922.
- Mazda, Y., Magi, M., Kogo, M., and Hong, P. N. (1997). Mangroves as a coastal protection from waves
- in the Tong King delta, Vietnam. *Mangroves Salt Marshes* 1, 127–135.
- 941 https://doi.org/10.1023/A:1009928003700.
- Mendez, F.J., Losada, I.J., (2004). An empirical model to estimate the propagation of random breaking
- and non-breaking waves over vegetation fields. *Coast. Eng.* 52, 103–118.
- 944 https://doi.org/10.1016/j.coastaleng.2003.11.003
- 945 Menéndez, P., Losada, I. J., Torres-Ortega, S., Narayan, S., and Beck, M. W. (2020). The Global Flood
- Protection Benefits of Mangroves. *Sci. Rep.* 10, 4404. https://doi.org/10.1038/s41598-020-61136-6.
- 947 Minikin, R.R. (1963). Winds, Waves, and Maritime Structures: Studies In Harbour Making and In the
- 948 Protection of Coasts, 2<sup>nd</sup> Edition. London, U.K. Charles Griffin and Company, ISBN
- 949 9780852640913, 0852640919
- 950 Mori N., Chang C.-W., Inoue T., Akaji Y., Hinokidani K., Baba S., Takagi M., Mori S., Koike H.,
- 951 Miyauchi M., Suganuma R., Sabunas A., Miyashita T., and Shimura T. (2022) Parameterization of
- 952 Mangrove Root Structure of *Rhizophora stylosa* in Coastal Hydrodynamic Model. *Front. Built*
- 953 Environ. 7:782219. https://doi.org/10.3389/fbuil.2021.782219
- 954 National Academy of Sciences (NAS). (1977). Methodology for calculating wave action effects
- 955 associated with storm surges. Washington, D.C. National Academy of Sciences.
- 956 National Oceanic and Atmospheric Administration (NOAA). (2015). Guidance for considering the use of
- 957 *living shorelines.* U.S. Department of Commerce. Washington, D.C.
- 958 Novitzky, P. (2010). Analysis of Mangrove Structure and latitudinal Relationships on the Gulf Coast of
- 959 *Peninsular Florida*. Ph.D. thesis. Florida, FL: University of South Florida.
- 960 Ohira, W., Honda, K., Nagai, M., and Ratanasuwan, A. (2013). Mangrove stilt root morphology modeling
- 961 for estimating hydraulic drag in tsunami inundation simulation. *Trees Struct. Funct.* 27, 141 148.
- 962 https://doi.org/10.1007/s00468-012-0782-8
- 963 Ostrow K.S. and Cox, D.T. (submitted) Performance-based Design Methodology for Nature-Based
- Solutions: Application to Using Mangroves to Mitigate Wave Overtopping. *Coastal Engineering*.
- 965 submitted.

- Ostrow, K., Guannel, G., Biondi, E.L., Cox, D.T., and Tomiczek, T. (2022). State of the Practice and
   Engineering Framework for Using Emergent Vegetation in Coastal Infrastructure. Frontiers in the
- 968 Built Environment.8, 2022, https://doi.org/10.3389/fbuil.2022.923965
- Park, H., Tomiczek, T., Cox, D.T., van de Lindt, J.W., and Lomonaco, P. (2017). Experimental modeling
   of horizontal and vertical wave forces on an elevated coastal structures. *Coastal Engineering*, 128
- 971 (2017) 58-74. http://dx.doi.org/10.1016/j.coastaleng.2017.08.001
- 972 Rahdarian, A., and Niksokhan, M.H. (2017). Numerical modeling of storm surge attenuation by
- mangroves in protected area of mangroves of Qheshm Island. Ocean Engineering, 145 (2017) 304-
- 974 315. https://doi.org/10.1016/j.oceaneng.2017.09.026
- Rosenberger, D., Marsooli, R. (2022). Benefits of vegetation for mitigating wave impacts on vertical seawalls. *Ocean Engineering*, 250, (2022). https://doi.org/10.1016/j.oceaneng.2022.110974
- 977 Sainflou, M. (1928). Treatise on vertical breakwaters. *Annals des Ponts et Chaussee*. Paris, France.
- 978 Tanimoto, K., Moto, K., Ishizuka, S., and Goda, Y. (1976). An investigation on design wave force
- 979 formulae of composite-type breakwaters. *Proceedings of the 23<sup>rd</sup> Japanese Conference on Coastal*
- 980 Engineering, pp. 11-16. (In Japanese). 981
- Tomiczek, T., O'Donnell, K., Furman, K., Webbmartin, B., and Scyphers, S. (2020a). Rapid Damage
   Assessments of Shorelines and Structures in the Florida Keys after Hurricane Irma. *Nat. Hazards Rev.* 21, 05019006. https://doi.org/10.1061/(ASCE)NH.1527-6996.0000349.
- 985 Tomiczek, T., Wargula, A., Lomónaco, P., Goodwin, S., Cox, D., Kennedy, A., and Lynett, P. (2020b).
- Physical model investigation of mid-scale mangrove effects on flow hydrodynamics and pressures
- and loads in the built environment. *Coast. Eng.* 162, 103791.
- 988 https://doi.org/10.1016/j.coastaleng.2020.103791.
- 989 Tomiczek, T., Wargula, A., O'Donnell, K., LaVeck, V., Castagno, K. A., and Scyphers, S. (2022).
- 990 Vessel-Generated Wake Attenuation by *Rhizophora Mangle* in Key West, Florida. *J. Waterw. Port*
- 991 *Coast. Ocean Eng.* 148, 04022002. https://doi.org/10.1061/(ASCE)WW.1943-5460.0000704.
- Tomiczek, T., Wyman, A., Park, H., and Cox, D.T. (2019). Modified Goda equations to predict pressure
- 993 distribution and horizontal forces for design of elevated coastal structures. J. Waterway, Port,
- 994 *Coastal, and Ocean Engineering.* 145 (6), https://doi.org/10.1061/(ASCE)WW.1943-5460.0000527
- 995 Turconi, L., Faccini, F., Marchese, A., Paliaga, G., Casazza, M., Vojinovic, Z., and Luino, F. (2020).
- Implementation of Nature-based Solutions for hydro-meteorological risk reduction in small
- Mediterranean catchments: the case of Portofino Natural Regional Park, Italy. Sustainability, 12 (3),
- 998 1240. https://doi.org/10.3390/su12031240
- 999 U.S. Army Corps of Engineers (USACE) (2002). *Coastal Engineering Manual*. Washington, DC: 1000 USACE.
- 1001 Van Dang, H., Park, H., Shin, S., Tomiczek, T., Cox, D.T., Lee, E., Lee, D., and Lomonaco, P. (2023).
- Physical model comparison of gray and green mitigation alternatives for flooding and wave force
- reduction in an idealized urban coastal environment. Coastal Engineering, 184
- 1004 https://doi.org/10.1016/j.coastaleng.2023.104339

1005 Wang, Y., Yin, Z., Liu, Y. (2020). Numerical investigation of solitary wave attenuation and resistance 1006 induced by rigid vegetation based on a 3-D RANS model. Advances in Water Resources, 146, 1007 103755. https://doi.org/10.1016/j.advwatres.2020.103755 1008 Wang, Y., Yin, Z., and Liu, Y. (2022a). Laboratory study on the drag coefficient for mangrove forests in 1009 regular waves. Ocean Engineering, 255 (2022) 111522. 1010 https://doi.org/10.1016/j.oceaneng.2022.111522 1011 Wang, Y., Yin, Z., Liu, Y. (2022b). Experimental investigation of wave attenuation and bulk drag 1012 coefficient in mangrove forest with complex root morphology. Applied Ocean Research, 118, 1013 https://doi.org/10.1016/j.apor.2021.102974 1014 Webb, B. M., Dix, B., Douglass, S. L., Asam, S., Cherry, C., Buhring, B. (2019). Nature-Based Solutions 1015 for Coastal Highway Resilience: An Implementation Guide. Federal Highway Administration, U.S. 1016 Department of Transportation, FHWA-HEP-19-042. Washington, D.C. 1017 Wiebe, D. M., H. Park, and D. T. Cox. (2014). Application of the Goda pressure formulae for horizontal 1018 wave loads on elevated structures. KSCE J. Civ. Eng. 18 (6): 1573–1579. 1019 https://doi.org/10.1007/s12205-014-0175-1. 1020 1021 World Bank (2017). Implementing nature-based flood protection: Principles and implementation 1022 guidance. Washington, DC: World Bank. http://hdl.handle.net/10986/28837 1023 Yin, Z., Li, J., Wang, Y., Wang, H., and Yin, T. (2023). Solitary wave attenuation characteristics of 1024 mangroves and multi-parameter prediction model. Ocean Engineering, 285 (Part 2) (2023) 115372. 1025 https://doi.org/10.1016/j.oceaneng.2023.11537 1026 Yin, Z., Wang, Y., Liu, Y., Zou, W. (2020). Wave attenuation by rigid emergent vegetation under 1027 combined wave and current flows. Ocean Engineering 213, 107632. 1028 https://doi.org/10.1016/j.oceaneng.2020.107632 1029 Yin, Z., Yang, G., Wang, Y., Qiu, Q., Jiang, X. (2024). Numerical simulations of breaking wave 1030 propagation through the vegetation on a slope based on a drag coefficient prediction model. Ocean 1031 Engineering, 291. 116440. https://doi.org/10.1016/j.oceaneng.2023.116440 1032 Zelt, J. A., and Skjelbreia, J. E. (1992). Estimating Incident and Reflected Wave Fields Using an 1033 Arbitrary Number of Wave Gages. Proceedings of the Coastal Engineering Conference, (pp. 777-1034 788). https://doi.org/10.1061/9780872629332.058 Zhang, K., Liu, H., Li, Y., Xu, H., Shen, J., Rhome, J., et al. (2012). The role of mangroves in attenuating 1035 1036 storm surges. Estuar. Coast. Shelf Sci. 102–103, 11–23. https://doi.org/10.1016/j.ecss.2012.02.021. 1037 Zhang, R., Chen, Y., Lei, J., Zhou, X., Yao, P., Stive, M.J.F., 2023. Experimental investigation of wave

attenuation by mangrove forests with submerged canopies. Coastal Engineering, 186, 104403.

https://doi.org/10.1016/j.coastaleng.2023.104403

1038

1039

1040

## **Appendix A Instrumentation Locations**

### 1042 Table A.1. Coordinates of instrumentation.

Sensor Name	Description	x (m)	y (m)	z (m)
WG1	Wire resistance wave gauge	13.98	-1.38	-
WG2	Wire resistance wave gauge	25.36	-1.33	-
WG3	Wire resistance wave gauge	28.68	-1.31	-
WG4	Wire resistance wave gauge	29.60	-1.33	-
WG5	Wire resistance wave gauge	30.52	-1.32	-
WG6	Wire resistance wave gauge	31.44	-1.32	-
WG7	Wire resistance wave gauge	32.04	-1.31	-
WG8	Wire resistance wave gauge	54.60	-1.33	-
WG9	Wire resistance wave gauge	55.81	-1.32	-
WG10	Wire resistance wave gauge	56.42	-1.32	-
WG11	Wire resistance wave gauge	57.33	-1.33	-
WG12	Wire resistance wave gauge	57.95	-1.33	-
WG13	Wire resistance wave gauge	65.17	-1.36	-
USWG1	Ultrasonic wave gauge	29.17	-1.27	-
USWG2	Ultrasonic wave gauge	39.76	0.00	-
USWG3	Ultrasonic wave gauge	43.42	0.00	-
USWG4	Ultrasonic wave gauge	50.73	0.00	-
USWG5	Ultrasonic wave gauge	55.37	-1.37	-
USWG6	Ultrasonic wave gauge	59.77	-1.52	-
PD18-1	PDCR1830 pressure gauge	35.89	-1.53	1.24
PD18-2	PDCR1830 pressure gauge	39.55	-1.53	1.24
PD18-3	PDCR1830 pressure gauge	43.10	-1.54	1.22
PD18-4	PDCR1830 pressure gauge	46.87	-1.53	1.23
PD18-5	PDCR1830 pressure gauge	50.52	-1.52	1.23
PD18-6	PDCR1830 pressure gauge	54.19	-1.51	1.23
ADV1*	Acoustic Doppler velocimeter	32.24	-1.40	1.25*
ADV2	Acoustic Doppler velocimeter	43.09	-1.43	1.40
ADV3	Acoustic Doppler velocimeter	43.09	-1.43	1.55
ADV4	Acoustic Doppler velocimeter	43.09	-1.43	1.72
ADV5	Acoustic Doppler velocimeter	43.09	-1.43	1.86
ADV6*	Acoustic Doppler velocimeter	57.83	-1.41	1.38*

<sup>\*</sup>For layout 1, ADV1 and ADV6 were positioned at vertical coordinate z = 1.52 m.

1048 Table A.2. Coordinates of instrumentation used to measure loads on test wall

Sensor Name	Description	x (m)	y (m)	z (m)	_
PD18-7	PDCR1830 pressure gauge	61.20	0.02	1.09	_
PD18-8	PDCR1830 pressure gauge	61.21	0.02	1.24	
PD18-9	PDCR1830 pressure gauge	61.21	0.02	1.43	
PD8-1	PDCR 830 pressure gauge	61.22	0.02	1.58	
PD8-2	PDCR 830 pressure gauge	61.22	0.01	1.77	
PD8-3	PDCR 830 pressure gauge	61.21	0.01	1.92	
PD8-4	PDCR 830 pressure gauge	61.21	0.01	2.11	
PD8-5	PDCR 830 pressure gauge	61.21	0.01	2.26	
PD8-6	PDCR 830 pressure gauge	61.21	0.01	2.44	
PD8-7	PDCR 830 pressure gauge	61.21	0.01	2.59	
PD8-8	PDCR 830 pressure gauge	61.21	0.02	2.85	
PD8-9	PDCR 830 pressure gauge	61.22	0.01	3.00	
PD8-10	PDCR 830 pressure gauge	61.22	0.01	3.20	
PD8-11	PDCR 830 pressure gauge	61.22	0.01	3.41	
PD8-12	PDCR 830 pressure gauge	61.22	0.01	3.61	

### Appendix B Measured Hydrodynamic Parameters and Wave-Induced Forces

1051

Table B.1. Ensemble-average H and T at Array 2, maximum positive and negative forces on wall, and standard deviations for regular wave cases.

Trial	Layout	h <sub>v</sub> (m)	<i>H</i> (m)	H̄ 95% CI (%)	<i>T</i> (s)	$\overline{F_+}$ (kN/m)	F <sub>+</sub> 95% CI (%)	$\overline{Z_{F+}}$ (m)	<del>F</del> _ (kN/m)	F_ 95% CI (%)	$\overline{Z_{F-}}$ (m)	$\overline{F}/\overline{F_+}$	$\overline{F_{+,N}}/\overline{F_{+,BL}}$	$\overline{F_{-,N}}/\overline{F_{-,BL}}$
TD 1-1 1	HD	1.85	0.329	4.4	2.52	3.47	3.4	1.216	-3.52	-4.4	0.978	1.01	0.86	0.85
TR-h1-1	LD	1.85	0.375	1.9	2.51	3.89	1.8	1.216	-3.65	-0.7	0.968	0.94	0.96	0.89
	BL	1.85	0.412	4.2	2.52	4.05	3.7	1.234	-4.12	-4.4	0.955	1.02	1.00	1.00
	HD	1.85	0.273	7.5	4.11	5.37	3.0	1.101	-3.47	-2.1	0.927	0.65	0.82	0.88
TR-h1-2	LD	1.85	0.326	7.0	4.13	6.09	6.9	1.118	-3.78	-9.8	0.926	0.62	0.92	0.96
	BL	1.85	0.341	6.8	4.12	6.58	7.2	1.127	-3.93	-8.8	0.910	0.60	1.00	1.00
	HD	1.85	0.589	6.3	2.54	6.02	8.6	1.245	-5.96	-3.1	0.932	0.99	0.78	0.79
TR-h1-3	LD*	1.85	0.667	15.6	2.54	6.73	15.0	1.183	-6.23	-11.9	0.918	0.93	0.87	0.82
	BL*	1.85	0.772	14.6	2.55	7.76	9.8	1.206	-7.56	-8.5	0.874	0.97	1.00	1.00
	HD	1.85	0.544	10.0	7.66	14.08	2.8	1.256	-4.01	-2.1	0.913	0.28	0.85	0.80
$TR-h1-4^+$	LD	1.85	0.550	7.0	7.65	15.27	1.8	1.261	-4.45	-2.5	0.900	0.29	0.92	0.89
	BL*	1.85	0.587	9.0	7.66	16.67	3.0	1.244	-4.98	-7.9	0.898	0.30	1.00	1.00
	HD	1.48	0.204	6.5	2.25	1.76	3.9	0.916	-1.81	-6.0	0.851	1.03	0.82	0.82
TR-h2-1	LD	1.48	0.245	6.3	2.25	1.94	4.6	0.928	-2.00	-5.3	0.840	1.03	0.90	0.90
	BL	1.48	0.259	5.1	2.26	2.14	4.3	0.940	-2.22	-2.8	0.812	1.04	1.00	1.00
	HD	1.48	0.207	3.8	3.65	2.70	4.2	0.825	-2.12	-1.8	0.793	0.79	0.83	0.85
TR-h2-2	LD	1.48	0.228	5.4	3.65	2.89	5.5	0.835	-2.32	-1.9	0.793	0.80	0.88	0.92
	BL	1.48	0.244	8.8	3.65	3.27	6.6	0.837	-2.51	-4.3	0.764	0.77	1.00	1.00
	HD	1.48	0.372	5.0	2.25	3.10	3.3	0.995	-2.79	-2.3	0.792	0.90	0.79	0.71
TR-h2-3	LD	1.48	0.459	8.7	2.27	3.57	8.1	0.964	-3.39	-9.3	0.761	0.95	0.91	0.86
	BL*	1.48	0.516	11.7	2.27	3.92	14.0	0.959	-3.94	-9.9	0.740	1.01	1.00	1.00
	HD	1.48	0.386	8.2	6.80	8.20	2.1	0.976	-2.21	-8.5	0.751	0.27	0.80	0.83
TR-h2-4	LD	1.48	0.414	7.2	6.80	9.17	0.8	1.023	-2.28	-2.1	0.726	0.25	0.89	0.85
	BL*	1.48	0.456	11.9	6.80	10.26	8.0	1.020	-2.68	-15.7	0.740	0.26	1.00	1.00
	HD*	1.48	0.430	27.8	3.77	6.46	9.9	0.899	-4.07	-10.5	0.732	0.63	0.83	1.17
TR-h2-5	LD*	1.48	0.456	37.5	3.75	7.64	18.1	0.972	-3.94	-14.8	0.729	0.51	0.98	1.13
	BL*	1.48	0.380	22.1	3.75	7.80	14.0	1.010	-3.49	-25.5	0.738	0.45	1.00	1.00
	HD*	1.48	0.488	40.3	6.78	15.36	19.3	1.179	-2.22	-23.0	0.709	0.14	0.80	0.73
TR-h2-6	LD*	1.48	0.485	34.2	6.88	16.09	35.2	1.218	-2.41	-20.9	0.687	0.15	0.84	0.80
	BL*	1.48	0.503	34.0	6.90	19.16	24.9	1.179	-3.03	-15.0	0.740	0.16	1.00	1.00
	HD	1.03	0.122	3.9	1.85	0.78	3.2	0.671	-0.70	-4.3	0.585	0.89	0.79	0.76
TR-h3-1	LD	1.03	0.146	6.2	1.85	0.90	6.4	0.678	-0.83	-6.3	0.578	0.91	0.91	0.90
	BL	1.03	0.173	4.0	1.86	0.99	2.7	0.665	-0.91	-2.8	0.550	0.92	1.00	1.00

	HD	1.03	0.125	5.5	3.00	1.10	4.5	0.602	-0.82	-3.3	0.542	0.74	0.77	0.80
TR-h3-2	LD	1.03	0.138	4.6	3.01	1.27	1.6	0.604	-0.91	-2.4	0.544	0.72	0.89	0.88
	BL	1.03	0.160	5.9	3.01	1.43	1.1	0.593	-1.03	-3.2	0.525	0.72	1.00	1.00
	HD	1.03	0.203	5.4	1.87	1.23	4.8	0.698	-1.12	-2.6	0.550	0.91	0.70	0.66
TR-h3-3	LD	1.03	0.254	13.6	1.89	1.51	9.2	0.710	-1.40	-2.9	0.533	0.93	0.85	0.83
	BL	1.03	0.312	11.9	1.88	1.76	3.9	0.689	-1.69	-6.9	0.502	0.96	1.00	1.00
	HD	1.03	0.240	12.5	5.70	3.51	4.5	0.664	-1.18	-7.9	0.518	0.34	0.66	0.69
TR-h3-4	LD	1.03	0.293	8.1	5.71	4.22	3.5	0.706	-1.42	-5.2	0.512	0.34	0.79	0.84
	BL	1.03	0.376	19.6	5.70	5.33	12.9	0.715	-1.70	-13.8	0.492	0.32	1.00	1.00
	HD*	1.03	0.267	11.2	4.11	3.38	4.9	0.663	-1.51	-8.4	0.517	0.45	0.73	1.11
TR-h3-5	LD*	1.03	0.318	40.1	4.10	3.71	38.1	0.674	-1.28	-28.5	0.526	0.35	0.81	0.94
	BL*	1.03	0.312	9.1	4.13	4.60	7.3	0.701	-1.36	-15.1	0.503	0.30	1.00	1.00
TR-h3-6	HD*	1.03	0.316	47.8	5.67	4.85	7.6	0.708	-1.11	-43.3	0.527	0.23	-	-
	LD*	1.03	0.439	16.2	5.69	5.33	5.4	0.729	-0.93	-28.6	0.538	0.17	-	-
TR-h3-7	HD*	1.03	0.380	11.9	6.00	4.92	4.0	0.716	-1.14	-4.8	0.532	0.23	0.78	1.17
	LD*	1.03	0.348	20.0	6.01	5.50	4.9	0.725	-0.85	-19.7	0.582	0.15	0.88	0.87
	BL*	1.03	0.383	50.1	5.20	6.27	16.8	0.736	-0.97	-52.3	0.585	0.16	1.00	1.00
	HD	0.73	0.077	4.5	1.56	0.44	1.5	0.486	-0.33	-1.3	0.388	0.76	0.79	0.73
TR-h4-1	LD	0.73	0.098	3.3	1.56	0.48	3.6	0.485	-0.38	-3.2	0.389	0.79	0.86	0.84
	BL	0.73	0.110	4.9	1.57	0.55	3.0	0.483	-0.45	-6.7	0.352	0.82	1.00	1.00
	HD	0.73	0.080	5.4	2.50	0.54	5.0	0.437	-0.37	-3.53	0.377	0.68	0.78	0.87
TR-h4-2	LD	0.73	0.092	3.7	2.49	0.62	3.6	0.438	-0.38	-3.8	0.374	0.61	0.90	0.89
	BL	0.73	0.100	5.3	2.51	0.69	3.5	0.432	-0.42	-5.5	0.337	0.62	1.00	1.00
	HD	0.73	0.128	9.2	1.57	0.62	10.7	0.490	-0.53	-9.6	0.375	0.86	0.62	0.63
TR-h4-3	LD	0.73	0.169	5.1	1.58	0.74	2.2	0.514	-0.67	-1.5	0.375	0.90	0.75	0.80
	BL	0.73	0.207	19.6	1.58	0.99	17.4	0.503	-0.84	-7.4	0.330	0.85	1.00	1.00
	HD	0.73	0.152	7.0	4.80	1.43	4.5	0.457	-0.65	-5.1	0.352	0.46	0.79	0.85
TR-h4-4	LD	0.73	0.192	10.4	4.80	1.63	12.0	0.465	-0.74	-9.1	0.352	0.46	0.91	0.97
	BL*	0.73	0.226	16.5	4.80	2.01	9.2	0.468	-0.90	-8.2	0.322	0.42	1.00	1.00
	HD*	0.73	0.143	20.7	3.42	1.17	16.6	0.428	-0.59	-18.0	0.359	0.50	0.78	0.80
TR-h4-5	LD*	0.73	0.169	45.4	3.42	1.31	20.7	0.434	-0.61	-22.0	0.354	0.46	0.87	0.83
	BL*	0.73	0.221	33.9	3.53	1.50	54.5	0.423	-0.73	-20.4	0.330	0.49	1.00	1.00
	HD*	0.73	0.145	15.8	4.77	1.81	4.8	0.462	-0.39	-7.7	0.379	0.21	0.84	0.70
TR-h4-6	LD*	0.73	0.183	34.3	4.77	1.95	25.7	0.468	-0.45	-56.0	0.388	0.23	0.91	0.82
	BL*	0.73	0.218	39.3	4.39	2.15	18.7	0.455	-0.56	-72.6	0.336	0.26	1.00	1.00
-												_		

<sup>\*</sup>wave breaking observed during trial

†nonzero pressures measured at topmost gauge

<sup>53</sup> 

### Manuscript to be summited to Nature-Based Solutions or Ocean Engineering

**Table B.2:** Measured wave heights and periods at Array 2 and corresponding representative forces on wall for random wave cases.

Trial	Layout	<i>h</i> <sub>ν</sub> (m)	H <sub>1/3</sub> (m)	T <sub>1/3</sub> (s)	<i>H</i> <sub>m0</sub> (m)	<i>T<sub>p</sub></i> (s)	F <sub>1/3+</sub> (kN/m)	F <sub>1/10+</sub> (kN/m)	F <sub>1/100+</sub> (kN/m)	F <sub>1/250+</sub> (kN/m)	$z_{F1/250+}$ (m)	F <sub>1/250</sub> - (kN/m)	$Z_{F1/250}$ (m)	$\frac{\left F_{1/250-}\right }{F_{1/250+}}$	$\frac{F_{1/250+,N}}{F_{1/250+,BL}}$	$\frac{F_{1/250-,N}}{F_{1/250-,BL}}$
-	HD*	1.85	0.488	5.47	0.507	7.56	10.69	14.27	19.37	20.87	1.285	-8.39	0.846	0.40	0.73	0.91
TI-h1-1+	HD*	1.85	0.529	5.32	0.552	7.56	11.60	15.41	20.15	21.77	1.416	-8.14	0.864	0.37	0.76	0.88
	LD*	1.85	0.569	5.26	0.602	7.33	13.19	17.74	23.73	24.80	1.408	-8.32	0.846	0.34	0.87	0.90
	BL*	1.85	0.638	5.41	0.676	7.59	15.39	21.33	28.25	28.55	1.366	-9.23	0.843	0.32	1.00	1.00
	HD	1.85	0.321	2.61	0.334	2.74	2.96	3.56	4.09	4.17	1.307	-4.97	0.961	1.19	0.57	0.67
TI 1 1 0	HD	1.85	0.372	2.69	0.380	2.76	3.46	4.30	5.64	5.94	1.412	-5.90	0.941	0.99	0.82	0.79
TI-h1-2	LD	1.85	0.418	2.64	0.430	2.68	3.98	4.92	6.34	6.99	1.663	-6.72	0.910	0.96	0.96	0.90
	BL*	1.85	0.450	2.74	0.461	2.78	4.17	5.21	6.78	7.27	1.425	-7.46	0.893	1.03	1.00	1.00
	HD*	1.48	0.366	5.03	0.384	6.43	6.42	8.14	9.52	9.75	1.000	-4.74	0.704	0.49	0.70	0.85
TI-h2-1	LD*	1.48	0.407	4.96	0.426	6.64	7.27	9.35	11.12	11.32	1.057	-5.10	0.690	0.45	0.81	0.91
	BL*	1.48	0.464	5.00	0.486	6.67	8.47	11.11	13.64	13.96	1.032	-5.59	0.665	0.40	1.00	1.00
	HD	1.48	0.235	2.44	0.242	2.39	1.82	2.22	2.81	2.88	1.013	-3.40	0.773	1.18	0.74	0.81
TI-h2-2	LD	1.48	0.261	2.42	0.270	2.46	1.99	2.49	3.30	3.60	0.979	-4.10	0.751	1.14	0.93	0.98
	BL	1.48	0.306	2.38	0.313	2.40	2.32	2.84	3.78	3.88	1.146	-4.20	0.744	1.08	1.00	1.00
	HD	1.48	0.372	3.80	0.400	3.83	4.38	5.17	6.15	6.69	0.946	-5.14	0.699	0.77	0.59	0.84
TI-h2-3	LD*	1.48	0.424	3.71	0.452	3.82	4.68	5.75	7.58	8.98	1.105	-5.56	0.664	0.62	0.79	0.91
	BL*	1.48	0.486	3.68	0.522	3.85	5.71	6.86	9.13	11.36	1.347	-6.14	0.649	0.54	1.00	1.00
	HD*	1.03	0.208	4.91	0.219	6.27	2.52	3.28	4.41	4.78	0.724	-1.77	0.494	0.37	0.63	0.74
TI-h3-1	LD*	1.03	0.232	4.60	0.245	6.29	2.99	3.92	5.28	5.67	0.733	-2.02	0.480	0.36	0.74	0.85
	BL*	1.03	0.279	4.45	0.296	5.85	3.57	4.87	7.12	7.64	0.890	-2.38	0.475	0.31	1.00	1.00
	HD	1.03	0.113	2.06	0.116	2.18	0.69	0.86	1.06	1.10	0.713	-1.05	0.556	0.96	0.73	0.67
TI-h3-2	LD	1.03	0.132	2.05	0.133	2.13	0.74	0.93	1.16	1.19	0.727	-1.26	0.538	1.06	0.79	0.80
	BL	1.03	0.154	2.00	0.157	2.11	0.84	1.07	1.41	1.50	0.660	-1.58	0.508	1.06	1.00	1.00
	HD*	1.03	0.203	3.24	0.212	3.48	1.65	2.08	2.63	2.68	0.669	-1.95	0.489	0.73	0.71	0.80
TI-h3-3	LD*	1.03	0.231	3.17	0.242	3.50	1.88	2.39	3.05	3.11	0.698	-2.13	0.484	0.68	0.82	0.87
	BL*	1.03	0.285	3.16	0.297	3.17	2.25	2.88	3.64	3.80	0.697	-2.44	0.459	0.64	1.00	1.00
TI-h4-1	HD	0.73	0.124	4.32	0.132	4.88	1.09	1.40	1.76	1.79	0.454	-0.78	0.345	0.43	0.61	0.74
	HD	0.73	0.123	4.20	0.133	4.91	1.11	1.41	1.77	1.81	0.454	-0.77	0.351	0.42	0.62	0.73
	LD	0.73	0.153	4.16	0.163	4.89	1.28	1.68	2.18	2.29	0.496	-0.90	0.333	0.39	0.79	0.85
	BL	0.73	0.181	4.05	0.193	4.87	1.52	2.05	2.78	2.92	0.522	-1.06	0.311	0.36	1.00	1.00
TI-h4-2	HD	0.73	0.066	1.78	0.067	1.92	0.35	0.44	0.51	0.52	0.496	-0.46	0.384	0.89	0.72	0.66
	LD	0.73	0.084	1.75	0.085	1.78	0.40	0.49	0.58	0.59	0.498	-0.52	0.382	0.88	0.82	0.74
	BL	0.73	0.104	1.72	0.105	1.67	0.45	0.57	0.70	0.72	0.513	-0.70	0.344	0.97	1.00	1.00
TI-h4-3	HD	0.73	0.123	2.73	0.131	2.84	0.80	0.94	1.19	1.28	0.486	-0.78	0.349	0.61	0.74	0.71
	LD	0.73	0.154	2.70	0.164	2.62	0.90	1.07	1.32	1.40	0.502	-0.91	0.337	0.65	0.81	0.83

# Manuscript to be summited to Nature-Based Solutions or Ocean Engineering

	BL	0.73	0.195	2.60	0.207	2.63	1.08	1.29	1.55	1.72	0.504	-1.10	0.305	0.64	1.00	1.00	
1059	*wave breaking	observed	during tr	ial													
1060	†nonzero pressures measured at topmost gauge																
1061																	